Available online at www.sciencedirect.com

ScienceDirect

Geochimica et Cosmochimica Acta 309 (2021) 171–190

Geochimica et Cosmochimica Acta

www.elsevier.com/locate/gca

Hydrogen isotope fractionation *inside* silicate melts and glasses studied by ^{1}H and ^{2}H MAS NMR spectroscopy – Molecular insights into deuterium exchange at the melt-fluid interface

Nico Kueter *, George D. Cody, Dionysis I. Foustoukos, Bjorn O. Mysen

Earth and Planets Laboratory, Carnegie Institution of Washington, 5241 Broad Branch Road NW, Washington DC 20015, USA

Received 7 November 2020; accepted in revised form 17 June 2021; Available online 25 June 2021

Abstract

Hydrogen isotope ratios (D/H) measured on geological samples are used to trace the pathways of water in magmatic and hydrothermal systems. Interpreting respective isotope data relies thereby on the theoretical and empirical constraints on hydrogen isotope fractionation. This study revisits a recently discovered hydrogen isotope fractionation effect between alkali-rich and alkali-poor regions within hydrous alkali silicate melts (Wang et al., 2015). In a series of experiments conducted at variable P-T-$X_{H2O,\ D2O}$ conditions, we studied this intramolecular isotope effect by ^{1}H and ^{2}H solid-state nuclear magnetic resonance (NMR) spectroscopy on quenched hydrous sodium tetrasilicate melts (Na_2Oś$4SiO_2$ with 1:1 H_2O and D_2O).

The results indicate a marked difference in the reactivity of the protonated and deuterated hydrous species. It is observed that c. 70% of deuterium concentrates as deuterated silanols (Si-OD) in proximity to the sodium cations in the silicate melt structure, while the remaining 30% occupy the Na-poor regions in the silicate melt in the form of Si-OD and presumably molecular water (HDO_m). This distribution remains nearly constant under all experimental conditions. In contrast, the concentration of protonated hydrous species (Si-OH, H_2O_m) in the Na-rich and -poor regions of the silicate melt varies as a response to changing experimental P-T-X_{H2O} and cooling rate, which is linked to common water speciation reactions taking place within the melt (Si-O-Si + H_2O_m = 2Si-OH). Previously considered insignificant, ^{1}H NMR indicates that the speciation equilibrium is sensitive to pressure and correlates positively with Si-OH concentration. The significantly different reactivity of the isotope substituted hydrous species results in large molecular variations in the D/H ratio inside the sodium silicate melt. Measured intramolecular hydrogen isotope fractionation yields a 2- to 9-fold (in average 3-fold) enrichment of deuterium in Na-rich depolymerized regions in the silicate network, which translates to intramolecular fractionations of $1000\ln(\alpha) = 400$ to 2200. Generally, intramolecular fractionation tends to increase when the melt evolves towards fluid-saturated conditions. The pre-concentration of deuterium in the depolymerized Na-rich regions of the silicate melt results in a higher local D/H ratio that may carry over when these regions disintegrate into a silicate saturated aqueous fluid. In this way, intramolecular isotope fractionation poses a potent way of enriching silicate saturated aqueous fluids in deuterium, potentially explaining previous experimental in-situ observations of large hydrogen isotope fractionations in the hydrous-melt – silicate-saturated fluid system. The observed affinity of deuterium to combine with alkali-associated silanols could comprise an important molecular sieving mechanism for deuterium that enhances the D/H fractionation between silicate-rich fluids (and hydrous melts) and

* Corresponding author.
E-mail address: nkueter@carnegiescience.edu (N. Kueter).

https://doi.org/10.1016/j.gca.2021.06.025

the surrounding host rock. Consequently, intramolecular hydrogen isotope fractionation in hydrous silicate melts and silicate-rich aqueous fluids may be a very effective deuterium filter acting in the deep geological water cycle.

Keywords: Silicate melt; Volatiles; Hydrogen isotope fractionation; NMR spectroscopy; Magma degassing

1. INTRODUCTION

The Earth's geological water cycle is indivisibly linked to the various magmatic processes that formed and sustained the geologically active surface of our planet. For example, Hadean zircons witness the early differentiation of hydrous silicate melts forming the first proto-continental crust and indicate the presence of an early hydrosphere (Harrison, 2009; Harrison et al., 2017). With the initiation of plate tectonics in the Neoarchean, felsic continental cores grew from the extensive differentiation of hydrous melts formed from the reaction of recycled hydrous surface material with mantle peridotite and ultramafic proto-crust (Shirey et al., 2008). A hydrous-magmatic cycle that, for at least 3.6 Ga, continuously shapes volcanic arcs, concentrates rare metals, and sustains the volatile cycle of elements and molecules important for life. Thus, our understanding of water storage, mobility, and reactivity in silicate melts is fundamental for our perspective of how water has influenced Earth's magmatic past and present.

The measurement of hydrogen isotope ratios, deuterium (D) to protium (H), on geological samples has proven to be an invaluable tool to unravel the pathways of water in geological space (Shaw et al., 2012; Peslier et al., 2017; Loewen et al., 2019). The fractionation of D during the magmatic degassing is of particular interest, as it allows for mass balance calculations that shed light on the recycling efficiency of subducted water and the hydrogen isotopic composition of crustal and mantle water (or hydrogen) reservoirs (e.g., Shaw et al., 2008; Kleine et al., 2020).

Studies focussing on the deep water cycle in magmatic settings rely on theoretically or empirically derived isotope fractionation factors between a degassed volatile phase and its magmatic origin. While theoretical calculations can predict equilibrium isotope fractionation to great accuracy for mineral and gaseous substances, things become much more complicated when condensed phases are involved, such as melts or liquids. Thus, empirical studies based on experimental or natural observations are required to constrain the magnitude of equilibrium isotope fractionation when condensed phases are involved. For light-element isotope systems other than hydrogen, the fractionation behavior is, thereby, to first-order temperature-dependent, and the influence of other physical parameters on the fractionation process is usually negligible. However, given the small atomic mass and size of hydrogen isotopes, additional isotope effects arise from pressure variation, molar volume, solvent chemistry, and quantum nuclear effects (Driesner and Seward, 2000; Horita et al., 2002; Van Hook, 2011; Horita et al., 2018). This complicates experimental approaches aiming to determine the hydrogen isotope equilibrium fractionation between phases, which can be further obscured by the high diffusivity of hydrogen isotopes that impose additional open system conditions and cause kinetic isotope effects (Richet et al., 1986; Roskosz et al., 2018; Kueter et al., 2020). The complexity of hydrogen isotope exchange reactions becomes apparent in the silicate melt–fluid system, where hydrogen isotopes find many bonding environments, each characterized by unique vibrational properties that determine the respective fractionation behavior. It has been demonstrated for homogeneous (fluid phase) and heterogeneous (fluid-mineral) equilibria that variations of physical and/or chemical parameters affect the isotope partitioning within condensed phases with consequences for the bulk fractionation of hydrogen isotopes with a second phase (Driesner and Seward, 2000; Foustoukos and Mysen, 2012; Horita et al., 2018).

That hydrogen isotope fractionations in hydrous magmatic systems are susceptible to varying P-T conditions was first described in in-situ hydrothermal diamond anvil cell experiments (HDAC) equilibrating silicate saturated fluids with sodium-aluminum-silicate melts (Mysen, 2013a, b; Dalou et al., 2015). In such experiments, the D/H fractionations are often several hundred permil larger than compared to hydrogen isotope exchange during magmatic degassing at ambient pressure (Richet et al., 1986; Dobson et al., 1989; Pineau et al., 1998). The first evidence for the fractionation of hydrogen isotopes between structural entities *inside* silicate melts/glasses was reported by Wang et al. (2015) from solid-state ^{1}H and ^{2}H magic angle spinning nuclear magnetic resonance (MAS NMR) spectroscopy on variably deuterated hydrous sodium tetrasilicate glasses. The finding of surprisingly large D/H fractionations between sodium-rich and -poor regions within the melt/glass ($R = (D/H)_{Na\text{-}rich}/(D/H)_{Na\text{-}poor} \sim 3.2$) was related to the highly increased hydrogen isotope fractionation in the silicate melt – fluid system observed in HDAC experiments (Dalou et al., 2015). A subsequent study by Le Losq et al. (2016) confirmed the isotope effect in quenched hydrous sodium tetrasilicate melts with varying water content and demonstrated its compositional dependence on lithium- and potassium-bearing tetrasilicate glasses, where fractionation factors were shown to correlate positively with the ionic radius of the cation. The present study aims to further explore and quantify this newly discovered isotope effect in P-T-X_{X2O} space. By employing ^{1}H and ^{2}H MAS NMR spectroscopy, we experimentally investigate the effect of intramolecular hydrogen isotope fractionation inside quenched sodium tetrasilicate melt and discuss the results by presenting working hypotheses from the perspective of changing water speciation, shifting glass transition temperature, and different reactivity of the hydrous species isotopologues. Throughout this text, we use the expression "X" as in X_2O_m and XO to denote

either H or D in molecular water (subscript "m") or a hydroxyl group (e.g., in silanol, Si-OX). X_2O_t refers to the total (i.e., initial) water content used in the experiments. The expression "hydrous species" summarizes OX and X_2O_m.

2. EXPERIMENTAL AND ANALYTICAL TECHNIQUES

2.1. Sample preparation and experimental protocol

Sodium tetrasilicate glass ("NS4", $Na_2Si_4O_9$) was synthesized from a 4:1 molar mix of spectroscopically high purity SiO_2 and Na_2CO_3 (previously dried at 110 and 300 °C, respectively). The powders were ground under ethanol in an agate mortar for 30 min and the mixture heated in a Deltech Box furnace to 1250 °C at a rate of 5° min^{-1} to inhibit violent degassing of the Na_2CO_3. After holding for 30 min, the melt was quenched to glass by manually immersing the bottom of the platinum crucible in a water bath. To ensure homogenization, the glass was re-ground and melted again, following the same synthesis protocol. The final NS4 glass was ground in ethanol for one hour, dried at 110 °C for >24 h, and stored in a vacuum desiccator until further use. Examination of the starting material with a JEOL JXA-8530 electron microprobe (20 nA beam current, 15 kV acceleration voltage, and 20 μm beam diameter) confirmed a homogeneous glass composition with a Na/Si ratio of 0.5 as expected from NS4 composition (Supplement materials).

All experiments were run in a solid-media high-pressure apparatus with ¾ inch talc-pyrex-MgO assemblies with a graphite furnace (Boyd and England, 1960; Kushiro, 1976). Before experimental runs, the MgO assembly parts were fired at 1000 °C and the rest baked at 110 °C overnight to reduce the amount of adsorbed water. Experiments were run in 10 × 4 mm (length × outer diameter) Pt capsules filled with NS4 glass and 8 wt% of a purified 1:1 D_2O - H_2O mix (plus 4 and 6 wt% for experiments in the water series). The amount of NS4 powder was calculated from the weight of the water injected in the capsule, assuring an accuracy of total weight fraction of better than 0.02 wt %. Capsules were sealed under a stream of argon with a PUK arc welder and subsequently immersed in acetone for at least 24 h to check for any leaks; any capsules gaining weight were discarded. Similarly, all preparation and steps were controlled by weighing to assure that no volatiles were lost from the experiment.

Pressure-series experiments were run at 1400 °C at 0.7, 1.0, 1.5, 2.0 and 2.5 GPa. Temperature-series experiments were run at 1200, 1300, and 1400 °C at a constant pressure of 1.5 GPa. The 1200 and 1300 °C experiments were held at 1400 °C for 15 min before cooling at 100 °C min^{-1} to the dwell temperature. Water-concentration series equilibrated NS4 with 4, 6, and 8 wt% water for two hours at 1.5 GPa and 1400 °C. The water-series dataset was complemented by a previously unpublished data point of hydrous NS4 with 5 wt% water (H_2O only), synthesized at 1400 °C and 1.5 GPa, and by ^1H MAS NMR data of Le Losq et al. (2015) for NS4 with 1, 3, and 6 wt% H_2O synthesized at 1450 °C and 1.5 GPa at 1.5 h equilibration time (no ^2H MAS NMR data available). Note that added experiments were conducted at the same high-pressure apparatus and likely yield the same quench rates as our experiments. Cooling-rate experiments were equilibrated at 0.7 GPa and 1400 °C before cooling at rates between 5 to 4100 ° C min^{-1}, starting at 0.7 GPa and 1400 °C. The temperature was controlled with S-type ($Pt\text{-}Pt_{90}Rh_{10}$) thermocouple with no pressure correction for the received voltage signal (EMF). Uncertainties on temperature and pressure are ±10 °C and 0.1 GPa, respectively (Mysen, 2007). Experiments were heated at a rate of 100 °C min^{-1} and equilibrated for 2 h. Rapid quenching was done by turning off the power, which resulted in reproducible cooling rates that are linearly approximated to 4050 ± 140 °C min^{-1} between 1400 and 400 °C and to 1240 °C ± 120 °C min^{-1} between 400 and 250 °C (Supplementary Fig. S1). Slower linear cooling rates ranged from 1750 to 5 °C min^{-1} and were controlled with a Watlow F4T thermocontroller, resulting in an accuracy of better than 0.5 °C min^{-1}. After each experiment, the capsules were thoroughly cleaned from the MgO pressure medium and then weighed. Experiments with weight deviations >1 mg were discarded. Negative weight deviations were rarely detected, indicating that diffusive hydrogen loss from the experiment is negligible. Diffusive hydrogen contamination (^1H, since most abundant) is possible because minute volumes of adsorbed water may be reduced from interaction with the graphite furnace. However, the minimal total weight gains of <0.2 mg indicate that hydrogen gain was limited and has no significant effect on the total D/H ratio and total water content. Most samples were analyzed directly after recovery from the capsules; the effect of longer sample storage times is briefly discussed below.

2.2. NMR analyses

Magic angle spinning nuclear magnetic resonance (MAS NMR) analyses were performed using a Varian-Chemagnetics Infinity 300 solid-state NMR spectrometer employing a static magnetic field of 7.05 T. Powder samples were loaded in ZrO_2 rotor probes (2.5 mm and 5.0 mm O. D. for ^1H and ^2H, respectively). ^1H MAS NMR spectra were obtained with manual control fast MAS probe at a spinning frequency ($\omega/2\pi$) of 22 kHz (drift is less than ±20 Hz). Background ^1H signal from outside the RF coil was suppressed by employing a DEPTH four pulse sequence. With respect to the ^1H signal, the rotor background is negligible (Supplement Fig. S2). Acquisition parameters are a ^1H 90° pulse length of 2.5 μs, a 10 s recycle delay to account for spin-lattice relaxation time for ^1H of ca. 2 s, and a 200 kHz spectral width. Per sample, a total of 8000 free induction decays (FID) were acquired and combined to a spectrum. The spectra were referenced to tetramethylsilane (TMS), defined as 0 ppm. However, we note that a slight displacement of the NMR probe caused a chemical shift for two experiments (Exp. 6-6940 and 12-6944). Therefore, we decided to internally reference the ppm scale of all ^1H and ^2H MAS NMR spectra to the sharp high-frequency peak at 15.7 ppm of Exp. 10-6942. Gener-

ally, the peak position (chemical shift) of the high-frequency signal is not affected by variations of any experimental parameters. Thus, it serves as an ideal anchor point for comparative studies on signal shifts and intensities.

To obtain complete ^{1}H-^{2}H homonuclear decoupling, ^{2}H MAS NMR spectra were acquired at a MAS frequency of 8 kHz (under computer control to ±1 Hz) with an excitation pulse width of 1.5 μs ($\omega_1/2\pi = 55.5$ kHz, 30° nutation angle) and a 30° tip angle to reduce the recycle delay to 5 s. The quadrupolar nature of the spin = 1 of deuterium inevitably creates a more complex ^{2}H MAS NMR spectrum compared with the spin = ½ spectrum of ^{1}H via MAS NMR. Therefore, a typical ^{2}H MAS NMR spectrum is characterized by multiple sharp spinning sidebands (spaced at the MAS frequency) spreading over the frequency range of the quadrupole interaction (Cody et al., 2020). Instead of fitting all spinning sidebands individually, a purely isotropic ^{2}H MAS NMR spectrum can be obtained by rotor-synchronized acquisition at a MAS frequency of 8 kHz, exactly matching the spectral width (8 kHz) while keeping the filter width to 400 kHz. This means that all of the spinning sidebands arising from the quadrupolar interaction are folded exactly one on top of another, yielding a purely isotropic D-NMR spectrum with the advantage of a substantial increase in the signal-to-noise ratio (Eckman, 1982; Ashbrook and Wimperis, 2005). A limitation of the isotropic ^{2}H MAS NMR spectrum is the loss of spinning sidebands that would yield information about deuterated water speciation (Cody et al., 2020). A total of 16,000 ^{2}H MAS NMR FIDs were acquired per sample. Spectral data can be found in the supplementary materials.

3. RESULTS AND DISCUSSION

3.1. Glass sample petrography

Glass shards were investigated using a petrographic microscope to identify any vesicle nucleation and other quench textures (Mysen, 2007) (Supplementary Fig. S3). Experiment 6-6940 (900 °C, 1.5 GPa) contains ca. 80 vol % euhedral quartz crystals in a glassy matrix (Supplementary Fig. S4), suggesting equilibration in the melt + quartz phase field at sub-liquidus conditions (Wu et al., 1993; Mysen, 2009). Except for experiment 17-6949, all glasses synthesized at 0.7 GPa are vesicle-rich, which indicates phase separation. This conclusion is substantiated by the observation that decreasing quenching-rates roughly correlate with increasing vesicle size (<7 μm diameter at rapid quench to <250 μm diameter at 5°/min). Experiment 17-6949 was quenched at 50 °C min^{-1} at constant 0.7 GPa and is devoid of microscopically visible fluid exsolution. Slow quench experiments are characterized by localized lamellar crystallization of the melt. Euhedral phenocrysts of quartz (c. 100 μm) are observed at the slowest quench rate (Exp. 23-6955, 5° min^{-1}; Supplementary Fig. S3), consistent with in-situ observations of quartz-growth in water-saturated NS4 melts at 600 °C and 0.7 GPa (Mysen, 2009). Glasses synthesized from melts dwelling at ≥1200 °C and ≥1.0 GPa are vesicle-free and devoid of quench textures and phenocrysts. Equilibration pressures affected the breaking behavior of the glasses, e.g., 0.7 GPa experiments appeared solid and broke conchoidally, while higher-pressure glasses shattered in sub-millimeter disks. This could qualitatively indicate the preservation of a compacted glass structure reacting to sudden pressure release (Richet et al., 2000; Wondraczek and Behrens, 2007).

3.2. NMR signals

Hydrogen NMR provides information on the local molecular structure of O-H(D) arrangements in the silicate network, i.e., molecular water, silanol, and hydrated metal-oxide compounds. Alkali cations (M) like Na^{+} modify the tetrahedral silicate network by shifting the disproportionation reaction

$$M_2O + Q^n + Q^m = 2M^{+} + Q^{n-1} + Q^{m-1} \quad (1)$$

to the right side, increasing the number of non-bridging oxygens (NBOs) available for charge compensation (n, m = 4–1, i.e., number of bridging oxygens (BO) in tetrahedron), and thus increasing the ratio between NBO to tetrahedrally coordinated cations (i.e., Si; NBO/T). It has been argued that alkali cations preferentially coordinate with NBOs causing the micro-segregation of the melt/glass into a highly polymerized alkali-poor silicate network (low NBO/T) separated by regions of alkali-rich depolymerized silicate network (high NBO/T), known as the *Modified Random Network* concept (MRN; Greaves, 1985) (Supplementary Fig. S5). Hydrogen NMR is too local to reveal such microdomains, but it distinguishes hydrogenated oxygen proximal or distant to a cation. It may thus indirectly reveal the MRN structure of the NS4 glass.

The ^{1}H and ^{2}H MAS NMR spectra of hydrous alkali silicate glasses are characterized by a characteristic double-peak shape (Figs. 1 and S6) with a low-frequency signal with an intensity maximum at 4–6 ppm (LF-signal) and a high-frequency signal at 13–16 ppm (HF signal). The complex asymmetric shape of the HF and LF signals (Fig. 1) reflect a composite of multiple underlying resonances; The chemical shift of those resonances relates to the covalent O-H (or O-D) distance (Eckert et al., 1987; Eckert et al., 1988; Cody et al., 2020), where a signal is shifted to higher frequencies with increasing O-X bond length, i.e., the hydrogen nucleus experiences less shielding from the oxygen's electron cloud (Fig. 2). Given the complex molecular structure of silicate glasses, numerous molecular interactions can cause subtle variations in the O-X length that broaden the HF and LF NMR signal. Important is the distinct presence of the HF and LF signal, which indicate two markedly different bonding environments for hydrogen in the glass. The HF signal is thereby clearly correlated to Na^{+} ions solvated by NBO in the silicate melt, as only the LF signal is present in alkali-free hydrous silicate glasses and in fully polymerized alumo-silicate glasses where NBO/T = 0 (e.g., Kohn et al., 1989; Cody et al., 2005, 2020; Xue, 2009; Wang et al., 2015). The MRN theory is very useful to understand this and following observations. We will therefore use the expressions *Na-rich (depolymerized) regions* and *Na-poor (polymerized) regions to* distinguish between O-X configurations in the silicate

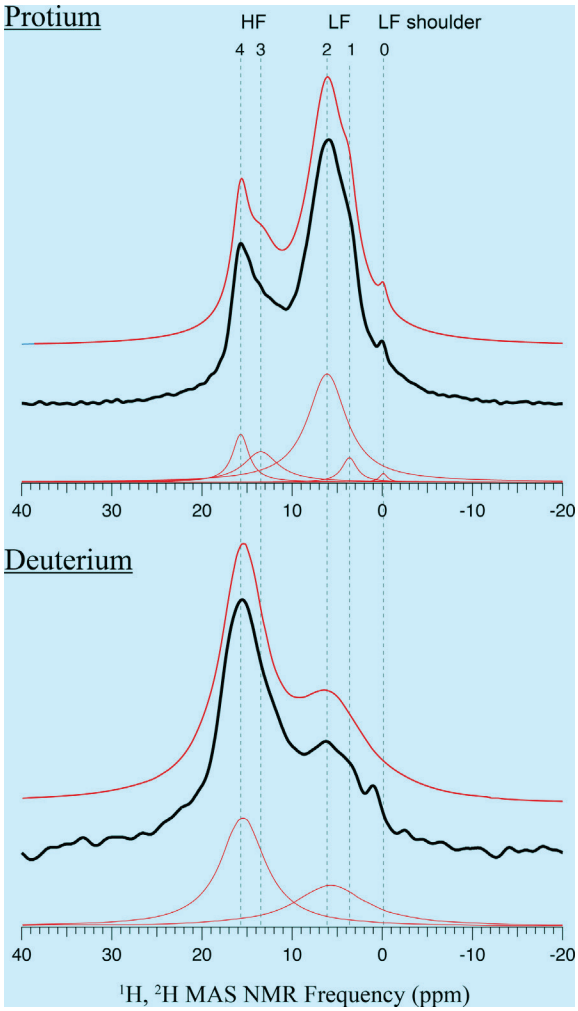

Fig. 1. Example of a typical ^{1}H and ^{2}H MAS NMR spectrum for hydrous sodium tetra-silicate glasses (NS4; black, top & bottom, respectively. Sample 4-6938). Both spectra show a characteristic double-peak center-band, where a minimum separates the respective high-frequency (HF) and low-frequency (LF) signals. The simulated ^{1}H MAS NMR spectrum (red curve, top panel) composes of five signals: 3.9 ± 0.2 and 6.1 ± 0.4 ppm for the LF signal (signal 1 & 2, assigned to Si-OX and X_2O_m in the Na-poor silicate network, respectively), 13.3 ± 0.3 and 15.7 ± 0.1 ppm for the HF signal (signal 3 & 4; Si-OX & X_2O_m and Si-OX in the Na-rich silicate network, respectively). An occasional shoulder peak is located between −0.2 to +0.7 ppm (signal 0; assigned to metal hydroxides, Na-OX). The ^{2}H MAS NMR is principally composed of the same underlying signals (dashed vertical lines) but is of much lower total intensity, inhibiting spectral simulation similar to the ^{1}H MAS NMR. Instead, the deuterium spectrum is satisfyingly simulated by two Lorentzian shapes (red curve, lower panel). (For interpretation of the references to colour in this figure legend, the reader is referred to the web version of this article.)

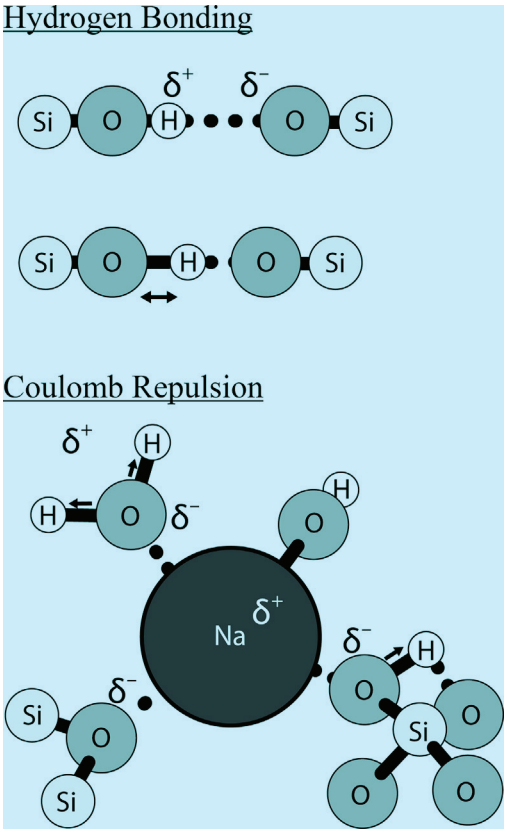

Fig. 2. Conceptual drawing of hydrogen variously bonded to oxygen in the silicate network as detected by hydrogen NMR. Chemical shifts correspond to the length of a covalent O-H (or O-D) bond. Deshielding of the hydrogen nucleus from the oxygen electron cloud (black arrow) shifts the signal to higher frequencies. Top panel: Deshielding in hydrogen-bonded settings is attained at reduced O-O distances, resulting from Coulomb attraction between hydrogen and acceptor oxygen (Eckert et al., 1988). This configuration has been proposed for the HF and LF signal (e.g., Wang et al., 2015), where the presence of a alkali-cation influences the HB bond length. Lower panel: Hydrogen nucleus deshielding as the result of Coulomb repulsion of positively charged hydrogen. For example, molecular water (top left) or NBO (silanol, bottom right). Intratetrahedral hydrogen bonding is indicated in the bottom right molecule (dashed line between H and O), as suggested by some workers for the 15.7 ppm resonance (see text). The low chemical shift of the LF shoulder signal indicates strong shielding of the hydrogen nucleus in a metal-hydroxide complex (top right). Na^{+} solvation is also possible by BO electron lone pairs (bottom left) but is not directly detectable via hydrogen NMR.

network that are interacting with cations (and thus have more NBO) and such that do not. We reiterate here, however, that hydrogen NMR spectroscopy cannot directly reveal the micro-segregation of alkali silicate melts, and the observed fractionation phenomena discussed below could also take place on much more local level.

Line shape modeling of the ^{1}H MAS NMR spectrum yields four underlying resonances at 3.9 ± 0.2 ppm and 6.1 ± 0.4 ppm for the LF signal and 13.3 ± 0.3 and 15.7 ± 0.1 ppm for the HF signal, and an irregularly appearing distinct shoulder on the low-frequency side of the LF signal between −0.2 to +0.7 ppm (Le Losq et al., 2015) (Fig. 1 top, details about the line shape modelling reported in the Supplementary Information). The ^{2}H MAS NMR spectrum is principally composed of the same underlying resonances, although the low signal intensity complicates satisfying modeling of the line shape using the above signal

positions (Fig. 1 bottom). Studies on alkali-free hydrous silica glass assign the 3.9 and 6.1 ppm signals to silanol (Si-OH) and molecular water (H_2O_m), respectively (Cody et al., 2020). The exact origin of the underlying 13 and 16 ppm resonance is debated but related to predominantly hydrated non-bridging oxygens (i.e., silanols) in the vicinity of alkali cations (Xue and Kanzaki, 2004). This region is nearly devoid of H_2O_m, as indicated by a lack of dipolar coupling visible as spinning sidebands (SSB) in the ^{1}H NMR spectra (Supplementary Fig. S6; Cody et al., 2005, 2020). The ^{2}H NMR spectra are the result of infolding the SSB, therefore direct information on the deuterium speciation cannot be retrieved. However, Wang et al. (2015) fit the full ^{2}H manifold of SSB and concluded that the HF region of the spectrum exhibited a classic Pake powder pattern with $\eta = 0$, consistent with a predominance of Si-OD, whereas the LF region exhibits both a classic pake pattern and a powder pattern with $\eta = 1$, consistent with the presence of both Si-OD and D_2O (and HDO) (Eckert et al., 1987). In other words, water close to alkali cations is mostly structurally bound to the silicate network in the form of Si-OX, while water in the silicate network unaffected by alkali cations is stored as X_2O and Si-OX.

Wang et al. (2015) interpreted the high-frequency ^{1}H NMR peak as being due to environments where O-H···O distances are close (e.g., Eckert et al., 1988, Xue and Kanzaki, 2004) (Fig. 2). Xue and Kanzaki (2001) suggested that the 13 ppm signal originates from a stronger hydrogen bonding environment for Si-OH and H_2O_m created by metal hydroxides (M-OH) acting as strong hydrogen acceptors. Robert et al. (2001) related the HF signal at 16 ppm to hydrogen bonding between Si-OH groups and NBO within silicate units (intratetrahedral hydrogen bonding, Fig. 2), based on the IR spectroscopic evidence of Mcmillan and Remmele (1986). Intratetrahedral hydrogen bonding was also suspected in hydrated crystalline sodium disilicate (Ai et al., 2002). Related, 15–16 ppm ^{1}H chemical shifts observed for hydrous sodium polysilicate phases (e.g., kanemite, magadiite, kenyaite) were linked to strong Si-O-H···O-Si hydrogen bonding between tetrahedral silicate layers that sandwich interlayers of Na^+ and water (Almond et al., 1997; Hayashi, 1997). However, alkalis can cause chemical shifts in the hydrogen spectrum similar to hydrogen bonding. Le Losq et al. (2015) showed that at equivalent total water concentrations, this peak was weak for LS4, moderate for NS4, and strong for KS4. This implies that the HF signal is correlated to the solvation Li, Na, and K by the silicate network, and larger ions require more oxygen lone pairs to compensate for coulomb repulsion between the alkali ions. Depolymerization of the silicate network provides silanol terminations that can supply oxygen lone pairs when H (and D) are moved away from the oxygen atoms they are bonded to (Fig. 2). Repulsed by the alkali's positive charge, this may result in the same level of chemical shift that the proximity of a neighboring oxygen atom might produce.

For the sake of simplicity, all following calculations and interpretation will be based on the total signal intensity of LF and HF signals. All hydrogen nuclei in the silicate network are excited equally by the NMR radio pulse, which renders the ^{1}H and ^{2}H MAS NMR signal intensity proportional to the hydrogen abundance. Thus, the relative abundance of hydrogen (i.e., hydrous species) in different structural regions within the glass structure is reflected by the intensity ratio of the LF and HF signals. We chose the HF signal intensity to express the relative proportion of hydrous species correlated to cations:

$$F^X_{HF} = \frac{I^X_{HF}}{I^X_{HF} + I^X_{LF}} \tag{2}$$

where I is the signal intensity of the annotated HF or LF signal, and X refers to the deuterium or proton NMR spectrum. The hydrogen isotope fractionation between Na-rich and Na-poor regions in the silicate melt (i.e., site affinity ratio) is expressed as:

$$R_{HF-LF} = \frac{(D/H)_{HF}}{(D/H)_{LF}} = \left(\frac{I^D_{HF}}{I^D_{LF}}\right) \cdot \left(\frac{I^H_{LF}}{I^H_{HF}}\right) \tag{3}$$

Experimental results are summarized in Table 1. Uncertainties in the R_{HF-LF} values are based on the on average factor 5 lower signal-to-noise ratio of the ^{2}H MAS NMR spectra and reported at 1σ level.

3.3. The effect of P-T-X_{X2O} and cooling rate on the hydrous NS4 structure

The speciation of water in silicate melts is controlled by the reaction:

$$X_2O_m + \text{Si-O-Si} = 2\text{Si-OX} \tag{4}$$

(X = D or H). Water in silicate melts directly influences the degree of polymerization of the tetrahedral network to the extent that the equilibrium moves to the right-hand side of the Q^n species disproportionation equilibrium (Eq. (1)). Near-infrared spectroscopy (NIR) studies suggest that the equilibria of Eqs. (1) and (4) are shifted to the left along a cooling and decompression path, stabilizing bridging oxygens (BO) and causing the formation of molecular water (X_2O_m) by condensing silanols (Si-OX) (Nowak and Behrens, 1995; Shen and Keppler, 1995; Zhang, 1999). It was shown, via NIR analysis, that the structure, and thus the water speciation in silicate glasses, will relax and re-equilibrate (and sometimes devitrify) along the cooling- and decompression path until the specific glass transition temperature (T_g) is reached (Dingwell and Webb, 1990) (Supplementary Fig. S9). Glass transition temperatures for the pressurized hydrous NS4 system are likely to be much less than 500 °C (see below; Mysen, 2009), but are strongly influenced by experimental pressure and temperature conditions, the water content of the melt, and the P-T path during cooling (Mysen and Richet, 2018). Accordingly, many of the experimental observations described below must be discussed with respect to variations in T_g. We thereby focus on the ^{1}H MAS NMR data first since it is the variability of the protons that gives rise to the isotope effects observed. We then discuss the constancy of deuteron speciation and present working hypotheses on the intramolecular isotope effect in the subsequent sections.

Table 1
Experiments and results. Uncertainties are 1σ.

Experiments						Signal Intensities				Signal Ratios				Chemical Shift (ppm)*				D/H Fractionation			
Run	T (°C)	P (GPa)	dwell (h)	cooling (min^{-1})	water (wt%)	^{1}H NMR		^{2}H NMR		^{1}H NMR		^{2}H NMR		^{1}H NMR		^{2}H NMR		R = (D/H)$_{HF-LF}$		1000ln(a)	
						LF	HF	LF	HF	HF/(LF+HF)	1σ	HF/(HF+LF)	1σ	ppm LF	ppm HF	ppm LF	ppm HF	R	1σ		1σ
Pressure series																					
12-6944	1400	0.7	2	rapid	8	0.11	0.03	0.03	0.08	0.20	0.002	0.70	0.02	4.0	13.1	3.6	13.1	**9.21**	0.12	**2220**	13
15-6947	1400	1	2	rapid	8	0.09	0.04	0.04	0.09	0.29	0.002	0.69	0.01	7.2	16.2	2.8	13.0	**5.48**	0.06	**1701**	10
10-6942	1400	1.5	2	rapid	8	0.07	0.05	0.04	0.08	0.41	0.01	0.69	0.01	6.4	15.8	3.1	13.3	**3.21**	0.04	**1166**	12
21-6953	1400	2	2	rapid	8	0.07	0.06	0.04	0.08	0.47	0.003	0.68	0.04	5.2	15.8	3.1	13.0	**2.35**	0.08	**853**	34
11-6943	1400	2.5	2	rapid	8	0.07	0.06	0.04	0.09	0.48	0.003	0.70	0.05	5.5	15.7	2.6	13.1	**2.57**	0.09	**943**	37
Temperature series																					
6-6940	900	1.5	2	rapid	8	0.08	0.04	0.03	0.09	0.36	0.002	0.72	0.04	3.7	13.1	3.6	12.6	**4.58**	0.11	**1522**	25
24-6956**	1200	1.5	2	rapid	8	0.06	0.06			0.48	0.002			5.4	15.8			***2.37***		***864***	
26-6958**	1300	1.5	2	rapid	8	0.06	0.05			0.47	0.01			5.2	15.6			***2.52***		***925***	
10-6942	1400	1.5	2	rapid	8	0.09	0.05	0.04	0.08	0.37	0.01	0.69	0.01	7.2	15.8	3.1	13.3	**3.86**	0.04	**1352**	11
Quench rate series																					
23-6955	1400	0.7	2	5	8	0.07	0.06	0.03	0.08	0.45	0.002	0.70	0.01	5.6	15.7	4.1	12.7	**2.80**	0.03	**1031**	12
5-6939	1400	0.7	2	10	8	0.08	0.05	0.04	0.09	0.40	0.003	0.70	0.04	5.9	15.7	3.3	13.3	**3.46**	0.11	**1243**	33
4-6938	1400	0.7	2	50	8	0.08	0.05	0.04	0.08	0.38	0.004	0.69	0.03	2.3	12.1	3.9	13.1	**3.67**	0.09	**1300**	23
17-6949 (iso)	1400	0.7	2	50	8	0.07	0.06	0.03	0.07	0.46	0.01	0.69	0.01	5.5	15.7	3.4	12.8	**2.66**	0.03	**978**	12
22-6954	1400	0.7	2	200	8	0.07	0.06	0.04	0.09	0.49	0.002	0.70	0.04	5.4	15.8	2.8	13.0	**2.44**	0.08	**892**	31
25-6957***	1400	0.7	2	1740	8	0.07	0.06	0.04	0.08	0.47	0.002	0.69	0.01	5.3	15.7			***2.53***	*0.03*	***928***	*12*
12-6944	1400	0.7	2	4100	8	0.11	0.03	0.03	0.08	0.20	0.002	0.70	0.02	4.0	13.1	3.6	13.1	**9.21**	0.12	**2220**	13
Water concentration series**																					
19-6951	1400	1.5	2	rapid	4	0.06	0.07	0.04	0.08	0.55	0.004	0.69	0.02	4.3	15.8			***1.83***	*0.03*	***606***	*16*
20-6952	1400	1.5	2	rapid	6	0.06	0.06	0.04	0.09	0.52	0.003	0.70	0.02	4.7	15.8	2.8	12.4	**2.14**	0.04	**759**	20
10-6942	1400	1.5	2	rapid	8	0.07	0.05	0.04	0.08	0.41	0.01	0.69	0.01	6.4	15.8	3.1	13.3	**3.21**	0.04	**1166**	12
UDP	1400	1.5	2	rapid	5	0.04	0.07	0.04	0.08	0.60								***1.52***		***416***	
Le Losq et al. (2015)	1450	1.5	1.5	rapid	1	0.05	0.12	0.04	0.08	0.70								***0.99***		***-10***	
Le Losq et al. (2015)	1450	1.5	1.5	rapid	3	0.05	0.08	0.04	0.08	0.60								***1.50***		***403***	
Le Losq et al. (2015)	1450	1.5	1.5	rapid	6	0.04	0.06	0.04	0.08	0.60								***1.53***		***424***	

Notes:
UDP = Unpublished data point.
* Chemical shift of the HF or LF signal maximum.
** Italic fractionation values calculated based on 2H MAS NMR data of experiment 10-6942.
*** Italic values based on 2H MAS NMR data averaged from the quench rate series experiments.
**** Italic values based on averaged 2H MAS NMR Data of Exp. 10-6942 and 20-6952.

3.3.1. Pressure

Water solubility in silicate melts increases with pressure and could be interpreted as the result of pressure-induced depolymerization of the silicate network (Stabilization of right side of Eq. (4)). While the positive relationship of pressure and water solubility is well studied, information on the pressure effect on Eq. (4) is scarce. No significant pressure sensitivity on the speciation equilibrium was reported from HDAC experiments, but the isochoric nature of these experiments makes it difficult to isolate pressure-from temperature effects (Shen and Keppler, 1995; Sowerby and Keppler, 1999; Chertkova and Yamashita, 2015). Piston cylinder experiments indicate the pressure stabilization of silanols with pressure in rhyolites (Hui et al., 2008).

Pressure stabilization of silanols should be reflected by a higher hydrogenated NBO (i.e., silanol) concentration detectable by hydrogen NMR. Indeed, a positive correlation of F^{H}_{HF} with pressure (Figs. 3a and 4a) is observed and indicates a systematic increase of the silanol concentration near sodium cations: F^{H}_{HF} rises from 0.2 at 0.7 GPa to 0.47 at 2.0 GPa. At >0.2 GPa, F^{H}_{HF} plateaus at 0.47 to 0.48. As visible from Fig. 3a, the rise of the HF signal is on expense of the LF signal, which also occurs to shift its maximum intensity from 6.7 to 5.4 ppm. This indicates a decrease of the H_2O_m component in the Na-poor silicate network and a concomitant increase of the Si-OH species in both, the Na-rich (mainly) and Na-poor (to a lesser degree) silicate network. Noteworthy is the decreasing slope and apparent plateauing of the F^{H}_{HF} value at >2.0 GPa (Fig. 4a) that suggests a saturation of the Na-rich silicate network in silanols.

Keeping in mind that structural relaxation will affect the melt until passing T_g (Dingwell and Webb, 1990), the observed systematics may reflect the silicate structure at the pressure present at T_g. We note here that the observed quench-induced pressure drop in our solid media pressure device is c. 0.4 ± 0.1 GPa and residual pressures at T_g may be approximated by subtracting this value from the dwell pressure. The effect of pressure on T_g in the hydrous NS4 system is, to our knowledge, not constrained. Generally, anhydrous alkali silicate glasses tend towards higher glass transition temperatures with increasing pressure, although the effect is small in the dry sodium silicate system (Wondraczek and Behrens, 2007). Assuming a similar behavior for the hydrous NS4 system, pressure-induced positive shifts would result in slightly elevated Si-OH concentrations. Thus, a positive correlation of T_g and pressure is at least qualitatively consistent with the increased F^{H}_{HF} values.

Remarkably, deuterated hydrous species yield nearly constant F^{D}_{HF} values of 0.69 ± 0.01, indicating a strong preference of deuterium for bonding environments near sodium cations (Figs. 3b and 4a). Fractionations become exponentially larger moving towards lower pressures, ranging from $R_{\text{HF-LF}} = 2.6$ at 2.5 GPa to $R_{\text{HF-LF}} = 9.2$ at 0.7 GPa (Fig. 4b), which is essentially the result of decreasing Si-OH stability towards lower pressures. The decompression-

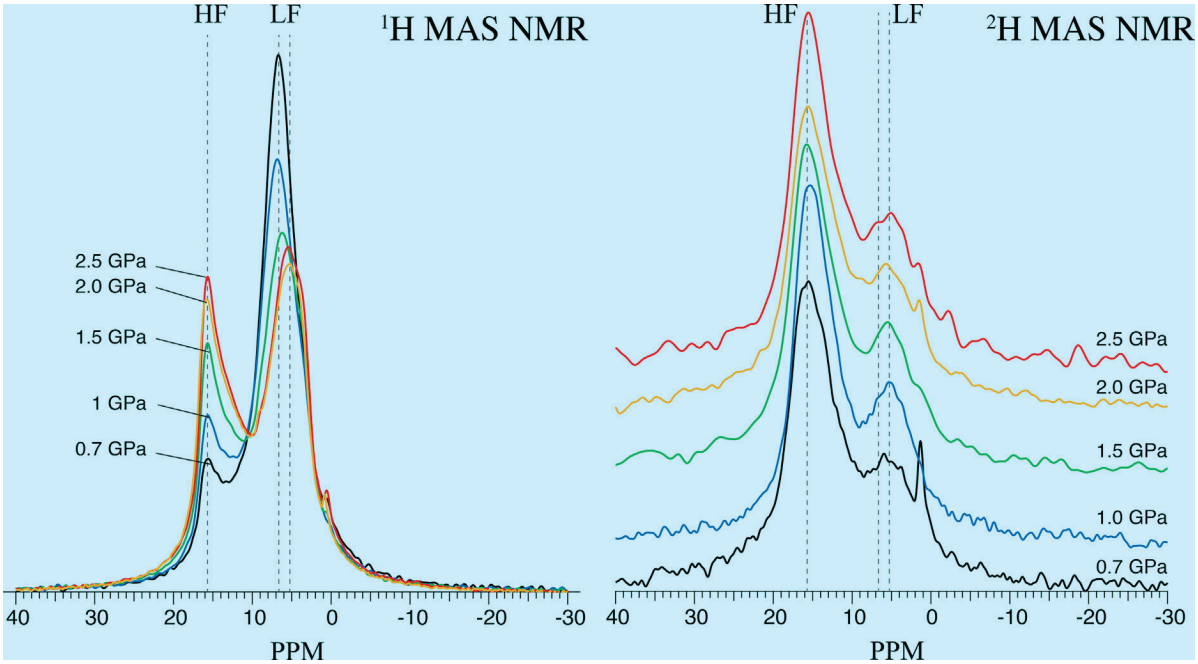

Fig. 3. Spectral variation observed in the ^{1}H and ^{2}H MAS NMR centerband with pressure. Visual comparison of the ^{1}H NMR spectra shows, with rising pressures, an increase in the HF signal and a decrease in the LF signal. The LF intensity maximum shifts with increasing pressure from 6.7 to 5.4 ppm due to a decreased contribution of the high-frequency component in the LF signal (maxima and shift indicated by dashed lines). In contrast, the ^{2}H NMR spectra show very little variation with pressure. The HF signal is constantly greater than the LF signal, indicating the preference of deuterium to concentrate in the sodium-rich silicate network. Dashed lines are located at the same chemical shift as in ^{1}H NMR spectrum and are shown for comparison.

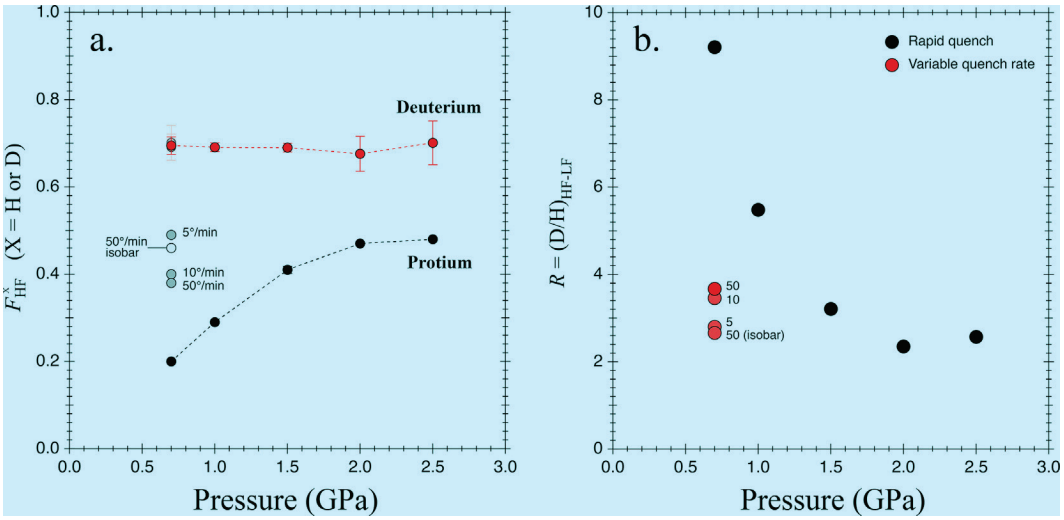

Fig. 4. Pressure series. (a) Relative intensity of the HF signal, expressed as F^X_{HF} (X = H or D, Eq. (2)) and shown for ^{1}H and ^{2}H MAS NMR (black and red symbols, respectively. Dashed lines are for eye guidance). Protium: F^H_{HF} correlates positively with pressure increasing from 0.2 to 0.48 and levels out at >2 GPa. Varying the cooling rate at 0.7 GPa results in systematically decreasing F^H_{HF} values (grey symbols, cooling rates annotated). Deuterium: F^D_{HF} shows no substantial variation with pressure. Variations in the cooling rate show no significant variation in the F^H_{HF}value (respective symbols hidden behind the red datapoint at 0.7 GPa). Note that c. 70% of deuterium accounts for the HF signal, while more than half of the protium accounts for the the LF signal. (b) Interstructural hydrogen isotope fractionation ($R_{HF\text{-}LF}$) as a function of pressure. For rapid-quench experiments, D/H fractionations decrease with pressure (black circles). Slowly quenched experiments yield markedly lower fractionations (annotated in °C min^{-1}). Uncertainties are within symbol size. (For interpretation of the references to colour in this figure legend, the reader is referred to the web version of this article.)

induced condensation efficiency for deuterated silanols appears to be much less than for protonated silanols given, as will be discussed in greater detail below.

3.3.2. Temperature series

The experimental temperature series was designed to constrain the isotope effect in temperature space, although following Dingwell and Webb (1990), it may be reasonable to expect no variations in the NMR spectra for the temperature series experiments. The applied dwell temperatures of 1200–1400 °C are effectively too high to allow for the quenching of the respective equilibrium melt structure (Supplementary Fig. S9). The rapid quench of the experiments likely resulted in the same cooling path and thus should, in theory, vitrify at a similar, much lower T_g. It is thus expected that the experiments yield a similar molecular structure, distribution of water, and water speciation. Indeed, the 1200 and 1300 °C experiments are very similar, as seen from the spectrum shape, and have almost identical F^H_{HF} values (0.48 and 0.47, respectively, Fig. 5). The underlying 6 ppm contribution to the LF signal of the 1400 °C experiment is significantly larger, lowering F^H_{HF} to 0.37 (Fig. 5). As apparent from the pressure series (Fig. 4a), this 1400 °C F^H_{HF} value is perfectly concordant with the 0.7–2.5 GPa experiments, suggesting that this apparent offset is real, and a curvilinear correlation between temperature and F^H_{HF} values exist in the temperature series. This negative temperature – F^H_{HF} relationship implies a decreasing concentration of hydrous species in the Na-rich regions of the silicate melt with increasing temperature. A possible explanation could be kinetically enhanced mean ionic distance between the Na^+ ions that would reduce the need for cationic shielding by NBO lone pairs because the Coulombic repulsion drops by $1/r^2$ (r = distance between ions). However, the current data set does not allow a satisfying constraint on the observed temperature effect of hydrous species migration, and more experiments are necessary.

A meaningful ^{2}H MAS NMR could only be measured for the 1400 °C experiment ($F^D_{HF} = 0.69 \pm 0.02$), because of a four-month delay in the ^{2}H MAS NMR analysis of the remaining samples because of the COVID-19 pandemic that resulted in degraded samples with strongly altered the deuterium spectra. This implies that hydrous NS4 glasses are not stable in the long term and degrade rapidly when stored at room temperature. A ^{2}H MAS NMR spectrum of a failed 900 °C experiment yields $F^D_{HF} = 0.72 \pm 0.04$, close to the 1400 °C F^D_{HF}-value. This qualitatively indicates no strong partitioning of deuterium as a function of temperature, with the peculiar effect that the intramolecular isotope fractionation increases with temperature due to the species reactions affecting Si-OH. As a result, fractionation factors, in part calculated by assuming a constant F^D_{HF} value of 0.69 (1400 °C experiment) range from $R_{HF\text{-}LF} = 2.4$ to 3.9 (Table 1).

3.3.3. Water content

Varying the total water content in an alkali silicate melt will distinctly influence its structural properties (Mysen and Richet, 2018). It is known that water suppresses the T_g significantly, especially at low total water contents (Deubener et al., 2003; Behrens and Yamashita, 2008). Accordingly,

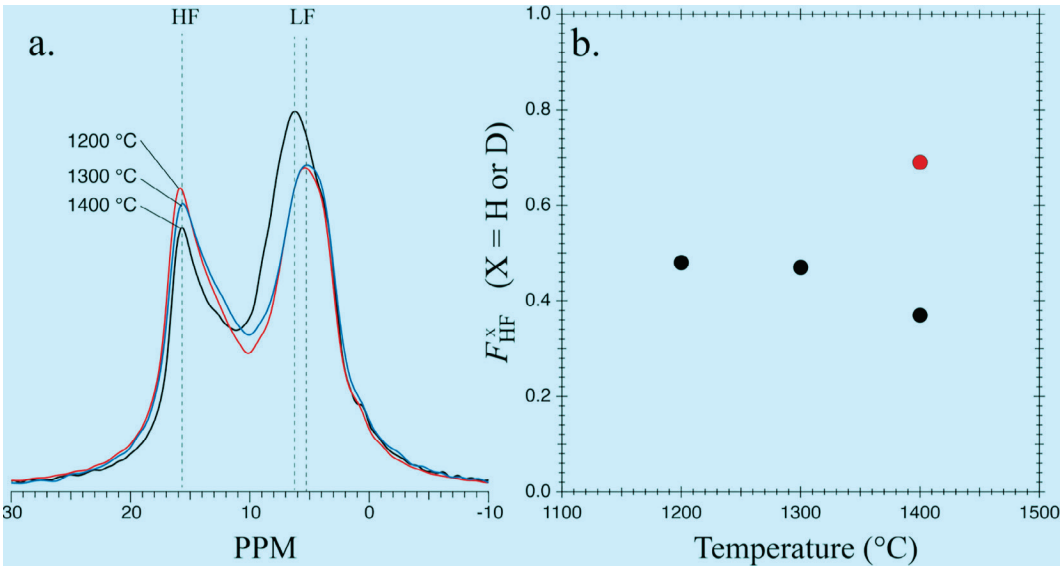

Fig. 5. Variations in the hydrous species distribution as a function of temperature. (a) Rising temperatures correlate with a decrease in the HF signal. The LF signal intensity and chemical shift of the LF signal maximum are similar for the 1200 and 1300 °C experiments. The 1400 °C experiment yields a higher LF intensity, which maximum is shifted from 5.2 to 6 ppm (maxima and shift indicated by dashed lines). (b) Relative intensity of the HF signal in the ^{1}H and ^{2}H MAS NMR spectra (black and red symbols, respectively). F^H_{HF} yield a slight curvilinear decrease with temperature. A F^D_{HF} value of c. 0.7 for the 1400 °C experiment shows that 70% of deuterium is associated with the HF signal. Uncertainties within symbol size. (For interpretation of the references to colour in this figure legend, the reader is referred to the web version of this article.)

strong variations in the hydrous species concentrations can be expected since the hydrous species equilibrium (Eq. (4)) would adjust until T_g is passed. Indeed, a linear decrease of the HF signal is observed ($F^H_{HF} = 0.7$ at 1 wt% to 0.41 at 8 wt% water; Fig. 6 including the data of Le Losq et al. (2015)), which indicates declining concentrations of silanols in Na-rich regions of the silicate melt. Interestingly, silanols in the Na-poor silicate network appear less affected by silanol condensation as the peak shape, and intensity of the 4 ppm contribution to the LF signal are nearly identical for 3–6 wt% experiments (Fig. 6a and Supplementary Fig. S7). The data are consistent with NIR speciation data on variably hydrous NS4 melts (1–5 wt% total H_2O, recorded *in-situ* at ambient pressure) reported by Behrens and Yamashita (2008), where the authors demonstrated that higher water contents resulted in lower T_g and a declining OH species fraction ($F_{OH,}$ Fig. 6c).[1]

NIR spectroscopy implies a drastic decrease in T_g for anhydrous NS4 at 480 °C to 320 °C at 1 wt%, and ~170 °C (extrapolated) at 8 wt% total water content and ambient pressure (Behrens and Yamashita, 2008). How the hydrous NS4 glass transition shifts as a function of water content and pressure is not constrained, but a positive linear correlation of T_g with increasing pressures has been demonstrated for anhydrous NS3, sodium borosilicate, and soda-lime silicate melts (Wondraczek and Behrens, 2007). Assuming a similar pressure response of anhydrous NS3 and hydrous NS4, extrapolation of the NS3 slope (25 °C GPa^{-1}) would then result in a T_g increase of 45 °C for the 1.8 GPa pressure interval in this study. However, a strong inverse pressure effect on T_g was suggested by Mysen (2009) for water-saturated NS4 melts in equilibrium with silicate-saturated fluids, lowering T_g for at least 200 °C for pressures up to 1.6 GPa, more consistent with the findings of Behrens and Yamashita (2008). Accordingly, a drop in T_g by c. 150 °C would mean that respective quench rates decrease from 1600 °C min^{-1} to just 400 °C min^{-1}, which theoretically prolongs the cooling interval by c. 10 s. This creates enough time for the re-equilibration of hydrous species to lower temperatures, i.e., the condensation of silanols to BO and formation of X_2O_m (Eq. (4)).

Despite the generally negative correlation of silanol concentration and total water content, the still relatively high F^H_{HF} values of >0.4 (Fig. 6c) indicate elevated silanol concentrations near the sodium cations; E.g., at 1 wt% total water content, 70% of all hydrogen is located in proximity to an alkali cation. This preference can be explained by the need for charge compensation and ionic shiedling (i.e. sovation) of sodium ions that is done by NBO (to which the hydrogen bonds to) and its electron lone pairs (Stebbins, 1987; Maekawa et al., 1991; Zotov and Keppler, 1998; Cody et al., 2005; Mysen and Richet, 2018). In the anhydrous NS4 system, where silica speciation consists of 50% Q^4 and Q^3 species (Maekawa et al., 1991; Zotov and Keppler, 1998), Na^+ charge compensation and solvation proceeds mostly by coordination with Q^3 NBOs (Baronnet and Rogez, 1987; Huang and Cormack, 1990, 1991; Gaskell et al., 1991; Farnan et al., 1992; Meyer

[1] We note that this estimate is based on the empirical calibration of Deubener et al. (2003), using hydrous species concentrations in hydrous glasses determined by NIR spectroscopy. The validity of NIR species determinations have been recently challenged in a comparative NIR-NMR study by Cody et al. (2020).

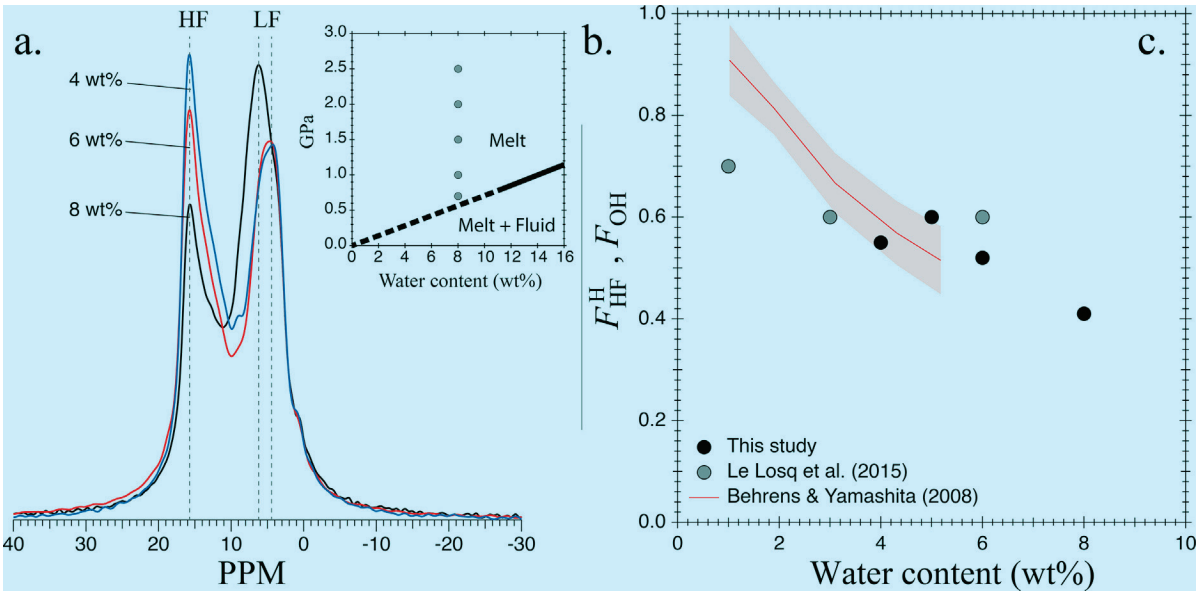

Fig. 6. Variations in hydrous species distribution as a function of the total dissolved total water content. (a) The HF signal intensity correlates negatively with total water content. Le Losq et al. (2015) reported a similar trend for experiments with NS4 glass containing 1, 3, and 6 wt% H_2O (see supplementary Fig. S7). The LF intensity maximum shifts from 4.5 to 6 ppm with increasing total water content. (b) Phase relationships in the hydrous NS4 system Mysen (2007). All experiments were run in the melt-only phase-field only; gray symbols show experimental pressures. Quenching resulted in a pressure decrease of about 0.4 ± 0.1 GPa per experiment. Experiments run at 1.0 GPa or higher quenched within the field, as petrographically confirmed by the lack of vesicles (see text). Experiments at 0.7 GPa experienced phase separation upon quenching (glass yields vesicles). Dashed line is the extrapolation of the fluid saturation surface from experimental data (solid line) for the hydrous NS4 system at 1100 °C by Mysen (2007). The fluid saturation surface is expected to shift by less than 0.1 GPa between 500 and 1400 °C based on thermodynamic calculations in the hydrous rhyolite system (Newman & Lowenstern 2002, not shown). (c) Relative HF intensity (F^{H}_{HF}) decreases with increasing total water content, broadly consistent with the decline in the OH-species fraction (F_{OH}) in hydrous NS4 reported by Behrens & Yamashita (2008) (red, shaded area = 1 σ uncertainty). Uncertainties within symbol size.

et al., 2004; Le Losq et al., 2017). Additional Na^+ solvation could be achieved with Si-O-Si oxygen lone pair electrons (Fig. 2). This would cause some lattice strain that is relaxed as water acts to form new NBOs which can substitute for Si-O-Si in solvation. The depolymerizing activity of water has the same effect as increasing the metal/Si ratio and thus provides ample configurations for Na^+ solvation by Q^3 and Q^2 species (Maekawa et al., 1991; Zotov and Keppler, 1998; Cody et al., 2005; Mysen, 2009). It appears that, at low total water contents, it is energetically more favorable for molecular water to depolymerize the Na-rich silicate network to form silanols that are then available for the solvation of alkali ions. This is also indicated by small or lacking HF spinning sidebands, which would indicate dipolar interaction between ^1H's in water molecules (Cody et al., 2020) present in a hydrous solvation shell existing around dissolved Na^+ ions (Hindman, 1962). Insufficient charge compensation by NBO at the lowest water concentrations can also explain the significantly increased LF shoulder peak as seen in the data Le Losq et al. (2015) (Supplementary Fig. S7). This signal was attributed to "free OH" (i.e., metal hydroxides without connection to the silicate network; Xue and Kanzaki, 2004), indicating that direct charge compensation of the cation by the formation of metal hydroxides becomes necessary due to the lack of available NBO.

The chemical shift of the LF intensity maximum from 5.5 to 6.5 at 8 wt% X_2O_t indicates the presence of a molecular water species (Fig. 6a, Supplement Fig. S7). This signal may result from the saturation of the Na-poor silicate network in silanols and increased storage of H_2O_m. Higher H_2O_m concentrations are also qualitatively indicated by increasing LF spinning sideband (Cody et al., 2005, 2020).

Notably, the distribution of deuterated hydrous species is not affected by the total water content; For all experiments F^{D}_{HF} averages to 0.69 ± 0.01. ^2H MAS NMR analyses of the 6 and 8 wt% samples show elevated HF intensities relative to the LF signal. Consequently, observed intramolecular D/H fractionation factors are due to the variability in the ^1H system. We calculated the fractionation factors for all experiments based on the averaged F^{D}_{HF} value above, assuming that the deuterium speciation is insignificantly affected by the water content. As seen from Fig. 7, the fractionation is largest for the 8 wt% H_2O_t experiment ($R_{HF\text{-}LF}$ = 3.2) and decreases linearly towards unity.

3.3.4. Cooling rate

The cooling rate of a melt determines the glass transition temperature and thus its effective temperature of last structural equilibration (Dingwell and Webb, 1990). Accordingly, hydrous speciation is dependent on the cooling rate.

The cooling-rate experiments were equilibrated at 0.7 GPa and 1400 °C, close to the fluid saturation surface of the hydrous NS4 system (Mysen, 2007; Fig. 6b). The cooling-induced decompression of the experiments by

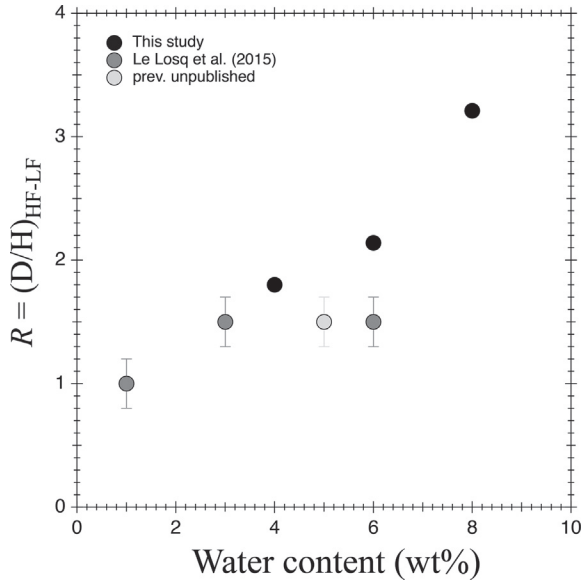

Fig. 7. Intramolecular hydrogen isotope fractionation ($R_{HF\text{-}LF}$) as function water content. Increasing total water contents correlate with higher $R_{HF\text{-}LF}$ values and could result from a drastically decreased glass transition temperature. Fractionation factors for literature and previously unpublished data are calculated based on the constant deuterium distribution observed in this study (see text).

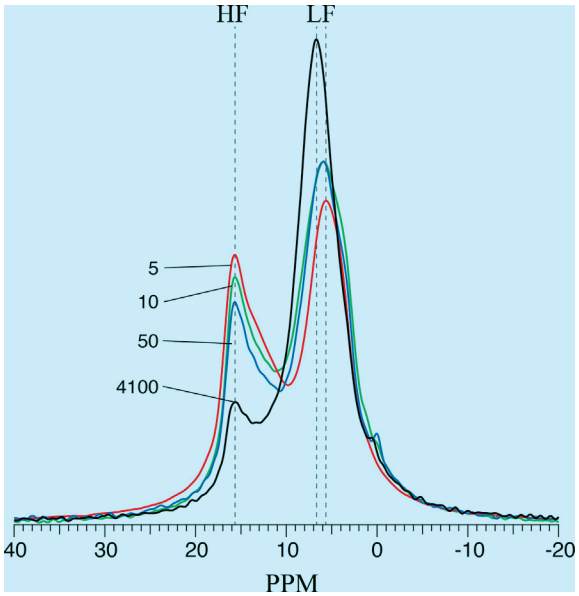

Fig. 8. ^{1}H MAS NMR spectrum of the quench-rate series (annotated in °C min^{-1}). Slower cooling rates correlate with increasing HF signal, decreasing LF signal, and a chemical shift of the LF intensity maximum from c. 6.5 ppm to 5.5 ppm. 200 and 1740 °C min^{-1} experiments are not shown for clarity because of post-experimental re-equilibration of the domain-specific water content (see Supplementary Fig. S8).

0.4 ± 0.1 GPa results in an overstepping of the fluid saturation surface and causes the degassing of a volatile phase, as evidenced by the occurrence of vesicles in the glass. Rapid quench produces lowest F^H_{HF} value of 0.2 that is concordant with those of higher-pressure rapid quench experiments (Fig. 4a). Such low F^H_{HF} values suggest that a high proportion of hydrous species is concentrated in the Na-poor regions of the silicate network, mostly in the form of H_2O_m, as indicated by the strong underlying high-frequency portion of the LF resonance (Fig. 8). Notably, all slow-quench experiments show elevated F^H_{HF}, implying that hydrous species increasingly concentrate in the Na-rich silicate network (Fig. 4a). Increasing F^H_{HF} values (0.2–0.49) and a chemical shift of the LF intensity maximum from 6.5 to 5.5 indicate the loss of H_2O_m from the Na-poor silicate melt structure. H_2O_m appears to take part in a depolymerization reaction in the Na-rich silicate network, where newly formed hydrated NBOs (i.e., silanols) are indicated by an increasing HF signal. This observation could be interpreted as cooling-induced phase separation/segregation, as outlined below. However, it appears unrelated to the observed fluid phase separation, as shown by the isobaric slow-quench experiment 17–6949 (cooled at 50° min^{-1}). This experiment yields a high F^H_{HF} of 0.46, similar to other non-isobaric slow-quenched experiments (Fig. 4a) but is lacking petrographic evidence for fluid exsolution, i.e., vesicles. Similar to the previous experimental series, F^D_{HF} remains invariable at 0.7 ± 0.01 (Supplementary Fig. S8). The resulting intramolecular fractionations tend to increase with increasing cooling rate from $R_{HF\text{-}LF}$ = 2.8 at 5° min^{-1} to 9.2 at rapid quench (Table 1). Again, this isotope effect is mainly due to variations in the proton speciation.

That the variation in the ^{1}H hydrous species is mainly the result of a low-temperature shift of T_g appears unlikely: Following Dingwell and Webb (1990), ΔT_g between the fastest and slowest quench amounts to only 20 °C (cf. Supplementary Fig. S9), that is too low to expect significant temperature-dependent variations in hydrous speciation and distribution. Instead, observed effects should rather be related to the subliquidus crystallization and near-T_g unmixing of amorphous NS4 and beginning devitrification (Klein et al., 1977; Baronnet and Rogez, 1987). Towards lower temperatures, the melt/glass attains an increasingly ordered molecular state, where the Na^+ in alkali-enriched regions can be expected to increasingly coordinate with Q^3 NBO to form periodic molecular arrangements that eventually could crystallize to hydrous sodium polysilicate hydrates of, for example, kanemite, kenyaite or magadiite type (Baronnet and Rogez, 1987; Heidemann et al., 1992; Almond et al., 1997; Hayashi, 1997; Zotov and Keppler, 1998). Such structures require silanol-bearing Q^3 species for charge compensation of the octahedral Na^+ interlayer (Almond et al., 1997). The increasing 16 ppm signal in the ^{1}H MAS NMR spectrum occurring with slower quench rates could thus show a higher silanol-terminated Q^3 component on the way towards a periodic arrangement and crystal nucleation. This interpretation is supported by the petrographic observation of lamellar birefringence pattern for 5 and 10 °C min^{-1} experiments that indicate profound devitrification of the glass matrix. Observed 15–16 ppm ^{1}H chemical shifts could then be attributed to strong Si-O-H···O$^-$-Si hydrogen bonding, connecting the tetrahedral

layer of sodium silicate phases (Almond et al., 1997; Hayashi, 1997).

3.3.5. Hydrous species reactions in the glassy state

Two "failed" experiments of the quench-rate series indicate the continuation of hydrous species reactions in the NS4 glasses: The 200 and 1740 °C min^{-1} quench rate experiments (22-6954 and 25-6957, respectively) yield the highest HF intensities and lowest LF intensities and thus do not follow the observed correlation of F^H_{HF} with quench rate (Supplementary Fig. S8). In fact, high F^H_{HF} values of in average 0.48 and low-frequency shifts of the LF intensity maximum resemble those of the slowest quench rate experiment (5 °C min^{-1}, $F^H_{HF} = 0.45$). This implies low-temperature reactions that continue to change the hydrous speciation in the NS4 glass. Contrary to all other experiments, these samples could not be measured for ^{1}H directly after the recovery from the capsule. Instead, the already powdered samples were stored for 4 and 9 days, respectively, at 110 °C before NMR measurement. Unexpected for these relatively low temperatures and short timescales, it appears that this storage was sufficient to cause species reactions within the NS4 glass. Therefore, these experiments were excluded from the dataset, but we report them to note that great caution should be taken regarding the sample storage (history) of hydrous alkali silicate glasses. Specifically, NMR studies should be performed nearly immediately after capsule opening.

4. DISCUSSION

4.1. Invariability of the ^{2}H MAS NMR spectrum

As outlined above, the distribution of deuterated hydrous species yields almost no variation with changing pressure, temperature, water content, and cooling rate. The apparent deuterium site preference, F^D_{HF}, averaged for all experiments is 0.7 ± 0.01, which is consistent with the experimental findings of Wang et al. (2015), where F^D_{HF} is ~0.7. In other words, the ^{2}H MAS NMR spectrum indicates that c. 70 % of deuterium atoms are associated with the NBO of silicate tetrahedra near sodium cations.

The invariability of the ^{2}H NMR spectra throughout the different experimental series is remarkable, especially if compared to the pronounced spectral variability of the proton spectrum, and points to a drastically different mobility and reactivity of the different hydrogen isotopes in the silicate melt. Thus, it is important to rule out any underlying issues in the acquisition of the ^{2}H MAS NMR spectra. Possible problems could arise from (i) insufficient or differential relaxation times (T_1) for the variously bonded deuterium after being excited by the radio pulse, and/or (ii) quadrupolar interactions. Regarding T_1-related issues, the question here would be whether differential T_1 saturation would distort the D-NMR spectrum relative to the ^{1}H NMR spectrum. Our set up of the experimental parameters uses recycle delays of 5 s (for D-NMR) and 10 s for ^{1}H NMR. Shorter recycle delays result in a reduction in the signal intensity due to T_1 saturation, however, no variation in the spectral intensities is observed indicating that the T_1's for the high frequency and low frequency bands are comparable. Consequently, T_1 effects are not the cause of the difference in HF/LF intensities with the D and H NMR, respectively.

Regarding the quadrupolar interaction, the spectral width of the rotational resonant acquisition of the D-NMR is only 8 KHz and signal acquisition was performed over a range of 400 KHz. The quadrupolar side bands extend out to ±100 KHz, however most of the intense sideband that disproportionally contribute to the rotational resonance ^{2}H NMR spectrum exist at ±50 KHz. Given the relatively low frequency for D on our NMR at 46.08 MHz, we are limited by our probe to a 90° pulse width of 4 μs, giving us a B_1 frequency of 62.5 KHz. Recognizing that the excited frequency range is a function of 90° pulse length, we know that all of the signal lies in the positive lobe of the sinc function frequency distribution spanning ±200 KHz of "on resonance". The purely zeroth order phase correction of the wide line spectra confirms no significant resonant offset phase issues. Most of the side band intensity is less than ±50 KHz so $\Omega/\gamma B1 < 1$ and the sideband signals are not diminished. The weak highest offset frequency side bands are at $\Omega/\gamma B1 = 1.6$ and will be slightly attenuated (to ~90% actual intensity). Such off-resonance effects would cause spectral distortion and systematically reduce the ^{2}H NMR 5 ppm LF signal relative to the HF signal by maximal 8%, provided that deuterons are purely rigid (Wang et al., 2015). This distortion is further reduced by a higher motional activity of deuterons (D_2O_m flipping, O-D vibrations) responsible for the LF signal, indicated by changes the asymmetry parameter from $\eta = 0$ (e.g. classic Pake powder pattern) to $\eta = 1.0$ (Eckert et al., 1987; Wang et al., 2015). As a consequence, the side band frequency spans the same range for quadrupolar coupling constants responsible for the LF and HF band, further reducing potential off-resonance effects.

We conclude that there are no underlying NMR issues that can explain why the ^{1}H NMR varies with experiments, but the ^{2}H NMR is essentially invariant. In fact, the ^{2}H NMR spectra are variable in chemically different systems. For example, Le Losq et al. (2016) showed decreasing ^{2}H LF intensities with increasing cationic size and Wang et al. (2015) reports a complex single, broadened signal for a deuterated haplobasaltic glass.

4.2. Deuterium enrichment in the Na-rich regions of the silicate melt

After excluding NMR-related issues, we are confident that the invariability of the ^{2}H spectrum is real, and as consequence any isotope effect observed results from the contrasting reactivity and mobility of deuterated and protonated species in the silicate melt.

Due to the large mass difference of hydrogen isotopes, OH and OD bonds in water and silanols yield markedly different vibrational properties. In the ground state, the variation in the vibrational zero-point energy (ZPE) defines the reduced isotope partition function ratios that describe

Table 2
Zero-point energies (ZPE).

Substance	ZPE		Reference
	cm^{-1}	kJ/mol	
OH	1851	22.14	Irikura (2007)
OD	1126	13.48	Irikura (2007)
H_2O	4504	53.88	NIST
HDO	3918	46.87	NIST
D_2O	3318.5	39.70	NIST

Rxn	ΣZPE (left)	ΣZPE (right)	ΔZPE (kJ/mol)
$H_2O + OD = HDO + OH$	67.35	69.01	−1.66
$HDO + OD = D_2O + OH$	60.34	61.84	−1.50

the fractionation behavior of substances (Bigeleisen and Mayer, 1947; Richet et al., 1977; Chacko et al., 2001; Schauble, 2004). Differences in the vibrational ZPE determine the direction of heavy isotope enrichment. This can be illustrated by the D/H exchange equilibrium between X_2O_m and OX (silanol):

$$H_2O_m + OD = HDO_m + OH \text{ and} \quad (5)$$

$$HDO_m + OD = D_2O_m + OH \quad (6)$$

The heavy isotope preference is predicted by summing the ZPE of the products and subtracting it from the summed ZPE of the reactant side of Eqs. (5) and (6) (Schauble, 2004), which yields ΔZPE of −1.66 and −1.50 kJ/mol (Table 2), respectively. As no ZPE for the O-X bond in silanol is available, the ZPE of silanols is approximated by hydroxyl (Irikura, 2007). The lower summed ZPE (ΣZPE) of the left side means that the deuteration of silanols is strongly favored as it minimizes the free energy of the system. Consequently, the generally lower ZPE of deuterated bond configurations predicts that a deuteron will preferably occupy a silanol over a proton. In turn, the energetic preference for deuterated silanols predicts that species reactions will predominantly affect the protonated species. Thus, the apparent D/H fractionation between Na-rich and -depleted regions in the silicate melt originates in the relatively higher reactivity of protonated hydrous species.

We defined the isotope exchange reaction between the Na-rich and -depleted silicate regions as $R_{HF\text{-}LF}$ (Eq. (3)). More generally, the hydrogen isotope fractionation factor between two substances A and B is defined as

$$\alpha_{A-B} = \frac{\left(\frac{D}{H}\right)_A}{\left(\frac{D}{H}\right)_B} \quad (7)$$

The fractionation factor $\alpha_{A\text{-}B}$ equals thereby $R_{HF\text{-}LF}$. The only difference is that $R_{HF\text{-}LF}$ does not describe D/H fractionation between two different substances A and B, but between two different hydrogenated structural entities in the tetrahedral silicate network, defined by the presence or absence of the sodium cations. In Fig. 9, this *intramolecular* fractionation is compared to hydrogen isotope fractionations in two-phase systems by expressing $R_{HF\text{-}LF}$ and α_{A-B} in the more conventional 1000ln(α) form, which at low fractionations approximates the δD fractionations measured in natural samples[2]. The intramolecular isotope fractionation is plotted at c. 200 °C as the best guess for the glass transition temperature. The underlying grey field is the T_g interval for NS4 glasses containing 3–8 wt% water (Behrens and Yamashita, 2008). As seen from Fig. 9, the intramolecular hydrogen isotope fractionation factors measured in our experimental samples are very large, ranging from 1.8 to 9.2 (1000ln(α) = 400–2220) and average at c. 2.8 ± 0.7 (excluding $R_{HF\text{-}LF} > 5$, n = 2; 1000ln(α) ≈ 1000 ± 250). These values are consistent with earlier findings of Wang et al. (2015) and Le Losq et al. (2016), reporting $R_{HF\text{-}LF} \sim 3.2 \pm 0.5$ (n = 5) and ~2.0 (n = 1). At high temperatures, equilibrium fractionations decline by c. $1/T^2$ towards unity (e.g., H_2O-H_2 fractionation curve in Fig. 9). This led Wang et al. (2015) to conclude that classical mass-dependent isotope fraction cannot explain such high intramolecular hydrogen isotope fractionations and instead suggested molar volume isotope effects (MVIE). However, as discussed earlier, quenching hydrous NS4 melts from 1400 °C (as in their study) is not possible as high water contents suppress the glass transition temperature to c. 250 °C or below, where D/H fractionations become larger (Fig. 9). However, MVIE are based on the different compressibility of isotope-substituted substances, and thus pressure variation could indeed affect their specific vibrational and fractionation properties (Polyakov and Kharlashina, 1994; Driesner, 1997; Polyakov et al., 2006). MVIE successfully predict experimental D/H fractionations in variously pressurized mineral-fluid systems, however, their effect is in the order of the second and third decimal place of $\alpha_{A\text{-}B}$ (Polyakov and Kharlashina, 1994; Horita et al., 2002; Polyakov et al., 2006; Horita et al., 2018). Thus, MVIE are unlikely to explain the large intramolecular hydrogen isotope fractionation.

The question remains whether the observed intermolecular isotope effect is of equilibrium or kinetic nature. Glasses have been interpreted to reflect the melt's structure at T_g, and thus the hydrous speciation may reflect the speciation at T_g as well (Dingwell and Webb, 1990; Deubener et al., 2003; Behrens and Yamashita, 2008). Isotopic equilibrium can only adjust after the melt's structural equilibration has been attained and the concentration of NBOs and X_2O_m has stabilized, allowing then for the diffusive exchange of hydrogen isotopes with respect to the equilibrium fractionation factor $\alpha_{A\text{-}B}$. Given the locality of species reactions, isotopic equilibration rates may be almost as fast as species reaction rates, assuming that species diffusion is not a reaction limiting factor. However, if longer diffusion pathways are required for silanols to find reaction partners, kinetic isotope effects (KIE) would be introduced due to the mass-dependent difference in diffusivity of the silanol isotopologues in favor of the lighter protonated silanol. Further, hydroxyl diffusion proceeds via the reaction of silanol with bridging oxygens (Behrens and Nowak,

[2] The δD notation describes the permil (‰) enrichment or depletion of a sample in deuterium relative to the Vienna Standard Mean Ocean Water (V-SMOW) defined at 0‰.

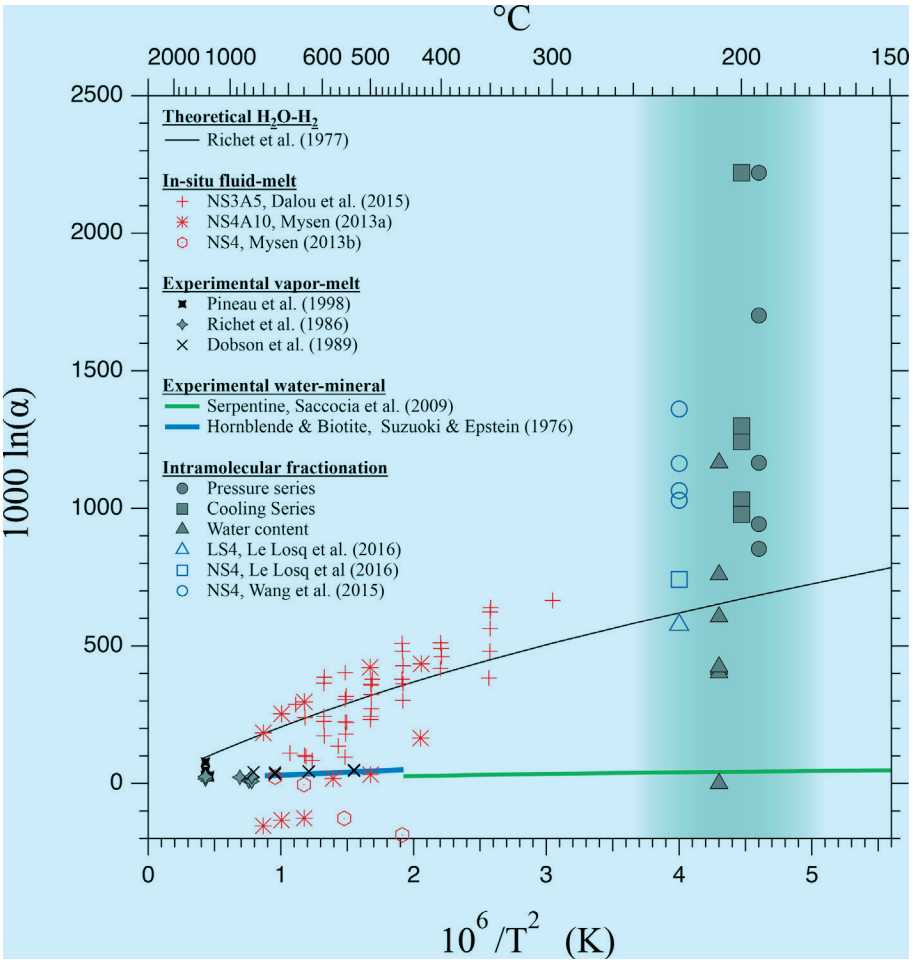

Fig. 9. Comparison of intramolecular hydrogen isotope fractionations observed in alkali silicate melts with theoretical, experimental, and natural hydrogen isotope fractionation factors. The intramolecular isotope fractionation in the hydrous alkali silicate melts is captured at the glass transition temperature (T_g). For hydrous NS4 glasses with 3 and 8 wt% total water content, the glass transition temperature interval is around 200 °C (upper and lower T boundary of the gray field; Based on Behrens & Yamashita 2008). Intramolecular fractionations are likely to fall within this temperature region. Corresponding symbols are plotted offset to another for better distinction and are not T_g estimates. Deuterium enrichment in the volatile phase during magmatic degassing and fluid-mineral reactions is in the order of few tens of permil (black and gray symbols, blue and green line). In comparison, D/H fractionations observed in-situ in the melt-fluid system are on average c. 3–5 times larger (red symbols). Note that the apparent fit of the theoretical fractionation curve for the water-hydrogen system (black curve) and the in-situ fluid-melt fractionation is coincidental. In-situ spectroscopic studies used the 2600 cm^{-1} and 3600 cm^{-1} Raman resonances for O-D and O-H Raman obtained from melt and fluid; resonances of molecular hydrogen were not considered. (For interpretation of the references to colour in this figure legend, the reader is referred to the web version of this article.)

1997), thus isotope effects on this diffusion mechanism would also be based on the reactivity of the isotopologues. Consequently, changes in the silanol diffusion rate and the silanol condensation rate itself could cause the relative kinetic enrichment of less reactive deutero-silanols in the silicate network because protonated silanols would react more readily. The kinetic isotope fractionation (α^{kin}) is then given by the ratio of the reaction rate constants:

$$\alpha^{kin} = \frac{k_i}{k_j} \tag{8}$$

where deviations from unity depict a kinetic enrichment or depletion of i relative to j during the reaction. The reaction constants $k_{i,j}$ denotes the unidirectional condensation reactions for isotope substituted silanols,

$$2Si - OH \overset{k_i}{\Rightarrow} Si - O - Si + H_2O \tag{9}$$

$$2Si - OD \overset{k_j}{\Rightarrow} Si - O - Si + D_2O \tag{10}$$

Above ΣZPE considerations suggest that $k_i > k_j$, supported by the highly variable F^H_{HF} values but nearly invariant F^D_{HF} values. A possible KIE may explain the very large intramolecular fractionations observed in the pressure series. Our ^1H NMR data suggest that protonated silanols are stabilized with pressure until a saturation limit is reacted above >2.0 GPa. As consequence, decompression (and temperature decrease) result in silanol condensation and formation of molecular water. Assuming a similar cooling path for all experiments, it is expected that the rate of silanol condensation is dependent on the initial equilibra-

tionpressure and decompression path, latter being nearly constant at 0.4 ± 0.1 GPa. Fig. 10 shows qualitatively that experiments quenched from high equilibration pressure (e.g., from 2.5 GPa to 2.1 GPa residual pressure) are expected to retain most of the silanols as result of a shallower slope $\left(\frac{\partial C_{Si-OH}}{\partial P}\right)$. Similarly, silanol condensation rates are expected to increase towards lower pressures, consistent with the observation that the system approaches the state of fluid saturation. As evident from Fig. 4a, the reaction of deuterated hydrous species is small in comparison, likely as the result of $k_i > k_j$. Consequently, at any given P, $\frac{\partial C_{Si-OD}}{\partial P}$ is expected to be shallower than $\frac{\partial C_{Si-OH}}{\partial P}$ with the result that always more Si-OH than Si-OD condense to form molecular water. Thus, the negative correlation of $R_{\text{HF-LF}}$ and pressure (Fig. 4b) stems from the higher condensation efficiency of Si-OH relative to Si-OD when cooled from different experimental dwell pressures. The observed pressure-related isotope effect is then probably of kinetic nature, but uncertainties remain as species equilibration may proceed very close to equilibrium due to the locality of the speciation reaction.

Above considerations would also apply to temperature effects upon cooling, as the speciation equilibrium (Eq. (4)) is known to stabilize silanols with temperature. As a consequence, it is possible that all D/H fractionations observed in the experiments yield a kinetic component introduced by the quenching process, that add to the equilibrium fractionation present at dwell temperature and pressure. If true, high-pressure experiments would then yield the closest approximation to an equilibrium intramolecular isotope effect, i.e $R_{\text{HF-LF}} \approx 2.5$.

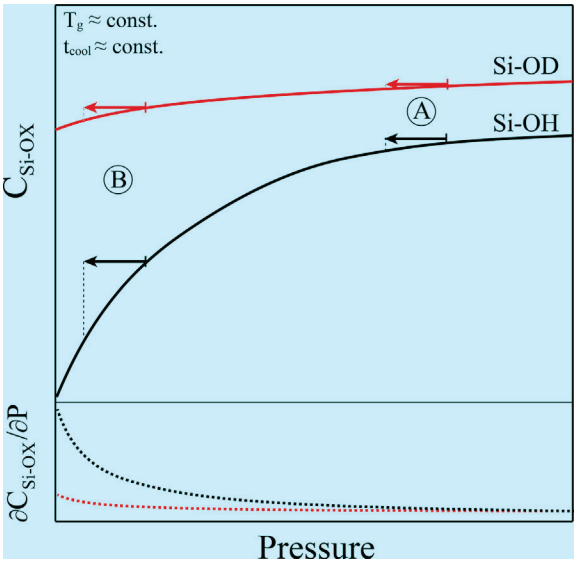

Fig. 10. Descriptive model on the pressure-dependency of silanols concentration (C_{Si-OX}). Respective first-order derivatives are displayed as dashed lines in the box below. Assuming a constant glass transition temperature (T_g), cooling interval (t_{cool}), and quenching-induced decompression of 0.4 GPa (arrows), the silanol condensation reaction $2Si\text{-}OX \rightarrow Si\text{-}O\text{-}Si + X_2O_m$ becomes less efficient when quenching from higher pressures. The overall efficiency of silanol condensation is larger for the Si-OH (black line) than for Si-OD endmember (red line). Case A: quenching from high pressure (e.g. 2.5 GPa) would cause only a minor decrease in the silanol concentration. Case B: Quenching from lower pressured (e.g., 0.7 GPa) will drastically decrease the Si-OH concentration but affect much less the deuterated silanols. (For interpretation of the references to colour in this figure legend, the reader is referred to the web version of this article.)

4.3. Geochemical implications

Intramolecular isotope effects in silicate melts could comprise an important fractionation mechanism in the deep water cycle. It is a peculiar fact that the isotopic composition of Earth's surface water is enriched in deuterium relative to the mantle's hydrogen reservoir. In δD notation, where Earth's current mean ocean water reservoir (VSMOW) is defined as 0‰, D/H measurements of mantle-derived materials yield consistently lower δD values (c. −60 to −80‰) (Lecuyer et al., 1998; Shaw et al., 2008). Various lines of evidence indicate that Earth's oceans have been enriched in deuterium over time, increasing the D/H ratio to its today's value (Pope et al., 2012; Kurokawa et al., 2018; Lecuyer et al., 2020). This enrichment has been linked to D/H fractionation during hydrogen loss via atmospheric VUV-photolysis reactions, serpentinization of oceanic lithosphere, as well as to billions of years of magmatic degassing. Fluid-mineral interactions and magmatic degassing tend to enrich deuterium in the volatile phases that can then efficiently recycle back to the surface hydrosphere. Typically, D/H fractionations amount to a few tens of permil deuterium enrichment in the volatile phase relative to the melt or mineral (Fig. 9; $1000\ln(\alpha) < 50$) (Suzuoki and Epstein, 1976; Richet et al., 1986; Dobson et al., 1989; Pineau et al., 1998; Saccocia et al., 2009). Interestingly, much larger D/H fractionations of up to several hundred permil have been observed in-situ via Raman spectroscopy between silicate saturated fluid and water-saturated sodium (aluminum) silicate melts (Mysen, 2013a, b; Dalou et al., 2015). This indicates that deuterium recycling may be about 3–5 times more efficient in the pressurized hydrous-melt – fluid system relative to the hydrogen isotope fractionation during magmatic degassing and mineral-fluid interaction at (near) atmospheric pressures. Our NMR data suggests that these large fractionations have their origin in the preconcentration of deuterium in the alkali-rich, depolymerized regions in the silicate melt structure. This preconcentration of deuterium in such regions is enhanced when the melt is decompressed or contains higher total water concentrations and is thus closer to fluid saturation (reflected by increasing $R_{HF\text{-}LF}$, Figs. 4 and 7). The actual transition from a fluid-saturated melt to a silicate saturated fluid is transient and proceeds by a continuous disruption of the polymeric silicate melt structure (Fig. 11; Mysen, 2013b). It is likely that, due to its highly depolymerized nature, alkali-rich regions continue to disintegrate and eventually exsolve as a silicate saturated aqueous fluid. This way, polymeric fragments may carry over their relatively high concentration of deuterium into the fluid phase while leaving behind a dryer, more polymerized and deuterium-depleted residual melt. Clearly, alkali-(Al)-Si glasses are

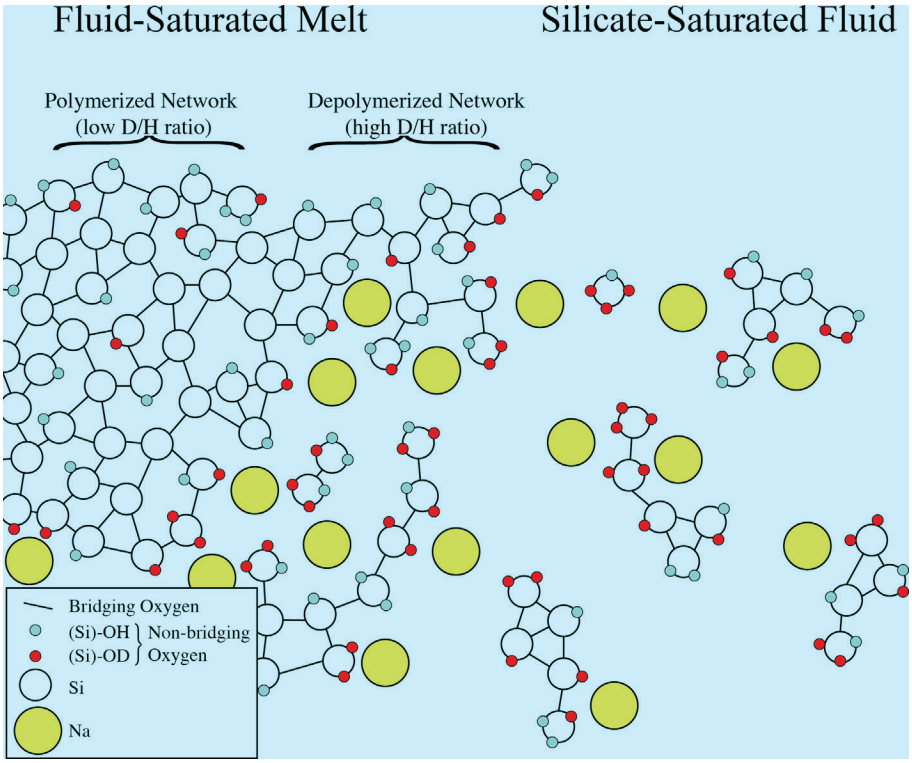

Fig. 11. Conceptual drawing of a hydrous silicate melt exsolving a silicate saturated aqueous fluid. Following the modified random network (MRN) theory, the melt structure consists of polymerized alkali-poor and depolymerized alkali-rich domains. Hydrogen NMR analysis shows the concentration of deuterium with the NBO coordinating alkali-cations, forming regions characterized by high D/H ratios. Further disintegration of these high-D/H depolymerized regions will form a silicate-saturated fluid exsolving from the remaining lower-D/H silicate melt. The pre-concentrated deuterium is then carried with the polymeric Si-Na fragments into the fluid phase (water molecules not displayed for simplicity).

highly simplified systems if compared to natural silicate melts, and it is unclear whether the presented concept (which is based on the MRN theory) is directly applicable to silicate melts undergoing fluid phase separation. However, Zotov et al. (1992) suggested locally polymerized microdomains that are separated by water-rich depolymerized regions in natural rhyolite. More recently, Le Losq et al. (2017) presented a more general model in which percolation channels and local alkali clusters are universal features in natural and synthetic silicate melts and glasses. In our system, NMR observations reveal alkali-NBO configurations as strong attractors for deuterium; It is not unlikely that this is also the case for highly depolymerized alkali-rich entities in more complex melt compositions. Indeed, despite the very complex shape of their ^{1}H and ^{2}H NMR spectra, Wang et al. (2015) report a possible intramolecular isotope effect in a peralkaline haplobasaltic glass.

A strong affinity of deuterium by Si-(Al)-alkali polymeric complexes could also have interesting consequences for hydrogen isotope fractionation beyond the magma-fluid interface. Hydrothermal fluids dissolve silicates and form Si-Al-alkali complexes (Mibe et al., 2008; Manning et al., 2010) that could attract deuterium from the aqueous solvent. A high D/H fractionation within the fluid between the dissolved polymeric species and the aqueous solute ($\alpha_{\text{polymeric species-water}}$) would then enhance the hydrogen isotope fractionation in the mineral-water system ($\alpha_{\text{water-mineral}}$). This is of particular interest for the mantle and lower crust, where fluid-rock interactions define the commonly very low D/H ratio of nominally anhydrous minerals (typically $\ll -80‰$; Bell and Ihinger, 2000).

5. CONCLUSIONS

Hydrogen isotope fractionation inside silicate melts is significant. Deuterium concentrates with non-bridging oxygens (NBO) that are solvating alkali-cations in the silicate melt structure. Within the silicate melt network, depolymerized alkali-rich regions tend to be separated from more polymerized alkali-poor regions, resulting in two structurally different domains characterized by very different D/H ratios. The D/H ratio of these regions is governed by the reactivity of the hydrated NBO, i.e., silanols (Si-OH or Si-OD). In both regions, deuterated silanols (Si-OD) are much less reactive than protonated silanols (Si-OH), and it is the higher reactivity of the latter that determines the D/H ratio of each structural region. Intramolecular hydrogen isotope fractionation, i.e., hydrogen isotope fractionation between both melt domains, is linked to hydrous speciation reactions in the melt, for example, the condensation of silanols to bridging oxygens and molecular water during cooling and/or decompression of the melt.

The high D/H ratio of the Na-rich depolymerized regions of the silicate melt may be carried over when these regions disintegrate to exsolve a silicate-saturated fluid, leaving behind a low-D/H polymerized melt. By this means, intramolecular isotope fractionation poses a potent mechanism for the enrichment of silicate-saturated fluids in deuterium. Such high-D/H fluids represent an efficient way to transport deuterium back to the Earths' surface and hydrosphere. Intramolecular hydrogen isotope fractionation in hydrous silicate melts and silicate-rich fluids may therefore constitute a very effective deuterium filter mechanism within the deep geological water cycle.

Declaration of Competing Interest

The authors declare that they have no known competing financial interests or personal relationships that could have appeared to influence the work reported in this paper.

ACKNOWLEDGMENTS

We thank Dr. Juliana Troch and Prof. Chris Huber at Brown University for valuable discussions. Joseph Lai and Caroline Beaumont are gratefully acknowledged for their laboratory support. Dr. Emma Bullock is thanked for EMPA help, and we are thankful for the library support of Shaun Hardy and Mary O'Donell. We gratefully acknowledge the helpful comments of three anonymous reviewers and the Associate Editor Prof. Sung Keun Lee, which improved the manuscript. The research was supported by a Carnegie Research Fellowship awarded to NK and by the W.M Keck Solid-State NMR Facility at Carnegie Earth and Planets Laboratory in Washington D.C. DF acknowledges the support provided by the NSF award EAR-1761388.

APPENDIX A. SUPPLEMENTARY MATERIAL

Supplementary data to this article can be found online at https://doi.org/10.1016/j.gca.2021.06.025.

REFERENCES

Ai X. J., Deng F., Dong J. X., Chen L. and Ye C. H. (2002) Stability of layered sodium disilicate during hydration process as studied by multinuclear solid state NMR spectroscopy. *J. Phys. Chem. B* **106**, 9237–9244.

Almond G. G., Harris R. K. and Franklin K. R. (1997) A structural consideration of kanemite, octosilicate, magadiite and kenyaite. *J. Mater. Chem.* **7**, 681–687.

Ashbrook S. E. and Wimperis S. (2005) Rotor-synchronized acquisition of quadrupolar satellite-transition NMR spectra: practical aspects and double-quantum filtration. *J. Magn. Reson.* **177**, 44–55.

Baronnet A. and Rogez J. (1987) Tem indication of amorphous phase-separation prior to disilicate nucleation in the $Na_2O{\cdot}2SiO_2$ supercooled liquid. *Chem. Geol.* **62**, 7–17.

Behrens H. and Nowak M. (1997) The mechanisms of water diffusion in polymerized silicate melts. *Contrib. Mineral Petr.* **126**, 377–385.

Behrens H. and Yamashita S. (2008) Water speciation in hydrous sodium tetrasilicate and hexasilicate melts: constraint from high temperature NIR spectroscopy. *Chem. Geol.* **256**, 306–315.

Bell D. R. and Ihinger P. D. (2000) The isotopic composition of hydrogen in nominally anhydrous mantle minerals. *Geochim. Cosmochim. Acta* **64**, 2109–2118.

Bigeleisen J. and Mayer M. G. (1947) Calculation of equilibrium constants for isotopic exchange reactions. *J. Chem. Phys.* **15**, 261–267.

Boyd F. R. and England J. L. (1960) Apparatus for phase-equilibrium measurements at pressures up to 50-kilobars and temperatures up to 1750 °C. *J. Geophys. Res.* **65**, 741–748.

Chacko T., Cole D. R. and Horita J. (2001) Equilibrium oxygen, hydrogen and carbon isotope fractionation factors applicable to geologic systems. *Stable Isotope Geochem.* **43**, 1–81.

Chertkova N. and Yamashita S. (2015) In situ spectroscopic study of water speciation in the depolymerized $Na_2Si_2O_5$ melt. *Chem. Geol.* **409**, 149–156.

Cody G. D., Ackerson M., Beaumont C., Foustoukos D., Le Losq C. and Mysen B. O. (2020) Revisiting water speciation in hydrous alumino-silicate glasses: a discrepancy between solid-state ^{1}H NMR and NIR spectroscopy in the determination of X-OH and H_2O. *Geochim. Cosmochim. Acta*.

Cody G. D., Mysen B. O. and Lee S. K. (2005) Structure vs. composition: a solid-state H-1 and Si-29 NMR study of quenched glasses along the Na_2O-SiO_2-H_2O join. *Geochim. Cosmochim. Acta* **69**, 2373–2384.

Dalou C., Le Losq C. and Mysen B. O. (2015) In situ study of the fractionation of hydrogen isotopes between aluminosilicate melts and coexisting aqueous fluids at high pressure and high temperature – implications for the delta D in magmatic processes. *Earth Planet Sci. Lett.* **426**, 158–166.

Deubener J., Muller R., Behrens H. and Heide G. (2003) Water and the glass transition temperature of silicate melts. *J. Non-Cryst. Solids* **330**, 268–273.

Dingwell D. B. and Webb S. L. (1990) Relaxation in silicate melts. *Eur. J. Mineral.* **2**, 427–449.

Dobson P. F., Epstein S. and Stolper E. M. (1989) Hydrogen isotope fractionation between coexisting vapor and silicate-glasses and melts at low-pressure. *Geochim. Cosmochim. Acta* **53**, 2723–2730.

Driesner T. (1997) The effect of pressure on deuterium-hydrogen fractionation in high-temperature water. *Science* **277**, 791–794.

Driesner T. and Seward T. M. (2000) Experimental and simulation study of salt effects and pressure/density effects on oxygen and hydrogen stable isotope liquid-vapor fractionation for 4–5 molal aqueous NaCl and KCl solutions to 400 °C. *Geochim. Cosmochim. Acta* **64**, 1773–1784.

Eckert H., Yesinowski J. P., Silver L. A. and Stolper E. M. (1988) Water in silicate-glasses - quantitation and structural studies by H-1 solid echo and mas-Nmr methods. *J. Phys. Chem.-Us* **92**, 2055–2064.

Eckert H., Yesinowski J. P., Stolper E. M., Stanton T. R. and Holloway J. (1987) The state of water rhyolitic glasses a deuterium Nmr-study. *J. Non-Cryst. Solids* **93**, 93–114.

Eckman R. R. (1982) *Hydrogen and Deuterium NMR of Solids by Magic Angle Spinning*. University of California, Berkeley, Berkeley.

Farnan I., Grandinetti P. J., Baltisberger J. H., Stebbins J. F., Werner U., Eastman M. A. and Pines A. (1992) Quantification of the disorder in network-modified silicate-glasses. *Nature* **358**, 31–35.

Foustoukos D. I. and Mysen B. O. (2012) D/H fractionation in the H-2-H_2O system at supercritical water conditions: compositional and hydrogen bonding effects. *Geochim. Cosmochim. Acta* **86**, 88–102.

Gaskell P. H., Eckersley M. C., Barnes A. C. and Chieux P. (1991) Medium-range order in the cation distribution of a calcium silicate glass. *Nature* **350**, 675–677.

Greaves G. N. (1985) Exafs and the structure of glass. *J. Non-Cryst. Solids* **71**, 203–217.
Harrison T. M. (2009) The Hadean crust: evidence from > 4 Ga zircons. *Annu. Rev. Earth Pl. Sc.* **37**, 479–505.
Harrison T. M., Bell E. A. and Boehnke P. (2017) Hadean zircon petrochronology. *Petrochronology: Methods Appl.* **83**, 329-+.
Hayashi S. (1997) Solid-state NMR study of locations and dynamics of interlayer cations and water in kanemite. *J. Mater. Chem.* **7**, 1043–1048.
Heidemann D., Hübert C., Schwieger W., Grabner P., Bergk K. H. and Sarv P. (1992) 29Si-und 23Na-Festkörper-MAS-NMR-Untersuchungen an Modifikationen des $Na_2Si_2O_5$. *Zeitschrift für anorganische und allgemeine Chemie* **617**, 169–177.
Hindman J. C. (1962) Nuclear magnetic resonance effects in aqueous solutions of 1–1 electrolytes. *J. Chem. Phys.* **36**, 1000–2000.
Horita J., Cole D. R., Polyakov V. B. and Driesner T. (2002) Experimental and theoretical study of pressure effects on hydrogen isotope fractionation in the system brucite-water at elevated temperatures. *Geochim. Cosmochim. Acta* **66**, 3769–3788.
Horita J., Driesner T. and Cole D. R. (2018) Hydrogen isotope fractionation in the system brucite-water +/- NaCl to elevated temperatures and pressures: implications for the isotopic property of NaCl fluids under geologic conditions. *Geochim. Cosmochim. Acta* **235**, 140–152.
Huang C. D. and Cormack A. N. (1990) The structure of sodium-silicate glass. *J. Chem. Phys.* **93**, 8180–8186.
Huang C. D. and Cormack A. N. (1991) Structural differences and phase-separation in alkali silicate-glasses. *J. Chem. Phys.* **95**, 3634–3642.
Hui H. J., Zhang Y. X., Xu Z. J. and Behrens H. (2008) Pressure dependence of the speciation of dissolved water in rhyolitic melts. *Geochim. Cosmochim. Acta* **72**, 3229–3240.
Irikura K. K. (2007) Experimental vibrational zero-point energies: diatomic molecules. *J. Phys. Chem. Ref. Data* **36**, 389–397.
Klein L., Handwerker C. and Uhlmann D. R. (1977) Nucleation kinetics of sodium disilicate. *J. Cryst. Growth* **42**, 47–51.
Kleine B. I., Stefansson A., Halldorsson S. A. and Barnes J. D. (2020) Impact of fluid-rock interaction on water uptake of the Icelandic crust: Implications for the hydration of the oceanic crust and the subducted water flux. *Earth Planet Sci. Lett.* **538**, 2.
Kohn S. C., Dupree R. and Smith M. E. (1989) A multinuclear magnetic-resonance study of the structure of hydrous albite glasses. *Geochim. Cosmochim. Acta* **53**, 2925–2935.
Kueter N., Schmidt M. W., Lilley M. D. and Bernasconi S. A. (2020) Kinetic carbon isotope fractionation links graphite and diamond precipitation to reduced fluid sources. *Earth Planet Sci. Lett.* **529**.
Kurokawa H., Foriel J., Laneuville M., Houser C. and Usui T. (2018) Subduction and atmospheric escape of Earth's seawater constrained by hydrogen isotopes. *Earth Planet Sci. Lett.* **497**, 149–160.
Kushiro I. (1976) A new furnace assembly with a small temperature gradient in solid-media, high-pressure apparatus. *Carnegie Inst. Washington Year Book* **75**, 832–833.
Le Losq C., Cody G. D. and Mysen B. O. (2015) Alkali influence on the water speciation and the environment of protons in silicate glasses revealed by H-1 MAS NMR spectroscopy. *Am. Mineral.* **100**, 466–473.
Le Losq C., Mysen B. O. and Cody G. D. (2016) Intramolecular fractionation of hydrogen isotopes in silicate quenched melts. *Geochem. Perspect. Lett.* **2**, 87-+.
Le Losq C., Neuville D. R., Chen W. L., Florian P., Massiot D., Zhou Z. F. and Greaves G. N. (2017) Percolation channels: a universal idea to describe the atomic structure and dynamics of glasses and melts. *Sci. Rep.-Uk* **7**.
Lecuyer C., Fourel F., Blamey N., Brand U. and Fralick P. W. (2020) delta-2-H of water from fluid inclusions in Proterozoic halite: evidence for a deuterium-depleted hydrosphere? *Chem. Geol.* **541**.
Lecuyer C., Gillet P. and Robert F. (1998) The hydrogen isotope composition of seawater and the global water cycle. *Chem. Geol.* **145**, 249–261.
Loewen M. W., Graham D. W., Bindeman I. N., Lupton J. E. and Garcia M. O. (2019) Hydrogen isotopes in high He-3/He-4 submarine basalts: primordial vs. recycled water and the veil of mantle enrichment. *Earth Planet Sci. Lett.* **508**, 62–73.
Maekawa H., Maekawa T., Kawamura K. and Yokokawa T. (1991) The structural groups of alkali silicate-glasses determined from Si-29 Mas-Nmr. *J. Non-Cryst. Solids* **127**, 53–64.
Manning C. E., Antignano A. and Lin H. A. (2010) Premelting polymerization of crustal and mantle fluids, as indicated by the solubility of albite plus paragonite plus quartz in H2O at 1 GPa and 350–620 °C. *Earth Planet Sci. Lett.* **292**, 325–336.
Mcmillan P. F. and Remmele R. L. (1986) Hydroxyl sites in SiO_2 glass – a note on infrared and Raman-spectra. *Am. Mineral.* **71**, 772–778.
Meyer A., Horbach J., Kob W., Kargl F. and Schober H. (2004) Channel formation and intermediate range order in sodium silicate melts and glasses. *Phys. Rev. Lett.* **93**.
Mibe K., Chou I. M. and Bassett W. A. (2008) In situ Raman spectroscopic investigation of the structure of subduction-zone fluids. *J. Geophys. Res.-Sol. Ea.*, 113.
Mysen B. (2013a) Effects of fluid and melt density and structure on high-pressure and high-temperature experimental studies of hydrogen isotope partitioning between coexisting melt and aqueous fluid. *Am. Mineral.* **98**, 1754–1764.
Mysen B. (2013b) Hydrogen isotope fractionation between coexisting hydrous melt and silicate-saturated aqueous fluid: an experimental study in situ at high pressure and temperature. *Am. Mineral.* **98**, 376–386.
Mysen B. O. (2007) The solution behavior of H_2O in peralkaline aluminosilicate melts at high pressure with implications for properties of hydrous melts. *Geochim. Cosmochim. Acta* **71**, 1820–1834.
Mysen B. O. (2009) Solution mechanisms of silicate in aqueous fluid and H_2O in coexisting silicate melts determined in-situ at high pressure and high temperature. *Geochim. Cosmochim. Acta* **73**, 5748–5763.
Mysen B. O. and Richet P. (2018) *Silicate Glasses and Melts*. Elsevier.
Newman S. and Lowenstern J. B. (2002) VOLATILECALC: a silicate melt-H_2O-CO_2 solution model written in Visual Basic for excel. *Comput. Geosci.-Uk* **28**, 597–604.
Nowak M. and Behrens H. (1995) The speciation of water in haplogranitic glasses and melts determined by in-situ near-infrared spectroscopy. *Geochim. Cosmochim. Acta* **59**, 3445–3450.
Peslier A. H., Schonbachler M., Busemann H. and Karato S. I. (2017) Water in the earth's interior: distribution and origin (vol 212, pg 743, 2017). *Space Sci. Rev.* **212**, 811.
Pineau F., Shilobreeva S., Kadik A. and Javoy M. (1998) Water solubility and D/H fractionation in the system basaltic andesite-H_2O at 1250 °C and between 0.5 and 3 kbars. *Chem. Geol.* **147**, 173–184.
Polyakov V. B., Horita J. and Cole D. R. (2006) Pressure effects on the reduced partition function ratio for hydrogen isotopes in water. *Geochim. Cosmochim. Acta* **70**, 1904–1913.

Polyakov V. B. and Kharlashina N. N. (1994) Effect of pressure on equilibrium isotopic fractionation. *Geochim. Cosmochim. Acta* **58**, 4739–4750.

Pope E. C., Bird D. K. and Rosing M. T. (2012) Isotope composition and volume of Earth's early oceans. *Proc. Natl. Acad. Sci. USA* **109**, 4371–4376.

Richet P., Bottinga Y. and Javoy M. (1977) Review of hydrogen, carbon, nitrogen, oxygen, sulfur, and chlorine stable isotope fractionation among gaseous molecules. *Annu. Rev. Earth Pl. Sc.* **5**, 65–110.

Richet P., Roux J. and Pineau F. (1986) Hydrogen isotope fractionation in the system H_2O liquid $NaAlSi_3O_8$ – new data and comments on D/H fractionation in hydrothermal experiments. *Earth Planet. Sc. Lett.* **78**, 115–120.

Richet P., Whittington A., Holtz F., Behrens H., Ohlhorst S. and Wilke M. (2000) Water and the density of silicate glasses. *Contrib. Mineral Petr.* **138**, 337–347.

Robert E., Whittington A., Fayon F., Pichavant M. and Massiot D. (2001) Structural characterization of water-bearing silicate and aluminosilicate glasses by high-resolution solid-state NMR. *Chem. Geol.* **174**, 291–305.

Roskosz M., Deloule E., Ingrin J., Depecker C., Laporte D., Merkel S., Remusat L. and Leroux H. (2018) Kinetic D/H fractionation during hydration and dehydration of silicate glasses, melts and nominally anhydrous minerals. *Geochim. Cosmochim. Acta* **233**, 14–32.

Saccocia P. J., Seewald J. S. and Shanks W. C. (2009) Oxygen and hydrogen isotope fractionation in serpentine-water and talc-water systems from 250 to 450 °C, 50 MPa. *Geochim. Cosmochim. Acta* **73**, 6789–6804.

Schauble E. A. (2004) Applying stable isotope fractionation theory to new systems. *Rev. Mineral. Geochem.* **55**, 65–111.

Shaw A. M., Hauri E. H., Behn M. D., Hilton D. R., Macpherson C. G. and Sinton J. M. (2012) Long-term preservation of slab signatures in the mantle inferred from hydrogen isotopes. *Nat. Geosci.* **5**, 224–228.

Shaw A. M., Hauri E. H., Fischer T. P., Hilton D. R. and Kelley K. A. (2008) Hydrogen isotopes in Mariana arc melt inclusions: implications for subduction dehydration and the deep-Earth water cycle. *Earth Planet. Sci. Lett.* **275**, 138–145.

Shen A. and Keppler H. (1995) Infrared spectroscopy of hydrous silicate melts to 1000 °C and 10 kbar: Direct observation of H_2O speciation in a diamond-anvil cell. *Am. Mineral.* **80**, 1335–1338.

Shirey S. B., Kamber B. S., Whitehouse M. J., Mueller P. A. and Basu A. R. (2008) A review of the isotopic and trace element evidence for mantle and crustal processes in the Hadean and Archean: implications for the onset of plate tectonic subduction. *Geol. Soc. Am. Spec. Pap.* **440**, 1–29.

Sowerby J. R. and Keppler H. (1999) Water speciation in rhyolitic melt determined by in-situ infrared spectroscopy. *Am. Mineral.* **84**, 1843–1849.

Stebbins J. F. (1987) Identification of multiple structural species in silicate-glasses by Si-29 NMR. *Nature* **330**, 465–467.

Suzuoki T. and Epstein S. (1976) Hydrogen isotope fractionation between oh-bearing minerals and water. *Geochim. Cosmochim. Acta* **40**, 1229–1240.

Van Hook W. A. (2011) Isotope effects in chemistry. *Nukleonika* **56**, 217–240.

Wang Y., Cody S. X., Foustoukos D., Mysen B. O. and Cody G. D. (2015) Very large differences in intramolecular D-H partitioning in hydrated silicate melts synthesized at upper mantle pressures and temperatures. *Am. Mineral.* **100**, 1182–1189.

Wondraczek L. and Behrens H. (2007) Molar volume, excess enthalpy, and Prigogine-Defay ratio of some silicate glasses with different (P, T) histories. *J. Chem. Phys.* **127**.

Wu P., Eriksson G. and Pelton A. D. (1993) Optimization of the thermodynamic properties and phase-diagrams of the Na_2O-SiO_2 and K_2O-SiO_2 systems. *J. Am. Ceram. Soc.* **76**, 2059–2064.

Xue X. Y. (2009) Water speciation in hydrous silicate and aluminosilicate glasses: direct evidence from Si-29-H-1 and Al-27-H-1 double-resonance NMR. *Am. Mineral.* **94**, 395–398.

Xue X. Y. and Kanzaki M. (2001) Ab initio calculation of the O-17 and H-1 NMR parameters for various OH groups: implications to the speciation and dynamics of dissolved water in silicate glasses. *J. Phys. Chem. B* **105**, 3422–3434.

Xue X. Y. and Kanzaki M. (2004) Dissolution mechanisms of water in depolymerized silicate melts: constraints from H-1 and Si-29 NMR spectroscopy and ab initio calculations. *Geochim. Cosmochim. Ac* **68**, 5027–5057.

Zhang Y. X. (1999) H_2O in rhyolitic glasses and melts: measurement, speciation, solubility, and diffusion. *Rev. Geophys.* **37**, 493–516.

Zotov N. and Keppler H. (1998) The influence of water on the structure of hydrous sodium tetrasilicate glasses. *Am. Mineral.* **83**, 823–834.

Zotov N., Yanev Y., Epelbaum M. and Konstantinov L. (1992) Effect of water on the structure of rhyolite glasses – X-ray-diffraction and Raman-spectroscopy studies. *J. Non-Cryst. Solids* **142**, 234–246.

Associate editor: Sung Keun Lee